Waste-to-wealth: biowaste valorization into valuable bio(nano)materials

Chunping Xu,[a±] Mahmoud Nasrollahzadeh,*[b±] Maurizio Selva,* Zahra Issaabadi[b], Rafael Luque*[cd]

Mankind is facing one of the most challenging turning points of his history, through the evolution of the current economy based on fossil sources to a new standard whereby both energy and daily use products and materials should be of renewable origin. This slow, but inexorable process to ensure life on Earth has already major implications in the handling of chemically rich bio-wastes, for example those coming from industrial and household food leftovers, which are processed for the preparation of basic chemicals, solvents, polymers, liquid and solid fuels, catalysts, adsorbents, functional and electrode materials. Under the umbrella of circular economy, the waste-to-wealth model is even a more general concept from the entrepreneurial standpoint, to promote a sustainable lifestyle where waste recycling is seen not only for its intrinsic benefits to the environment, but also to fuel profits in the creation of new technologies, livelihoods and jobs. Among keys for the success of this approach, it is imperative to develop affordable methods and socio-economic incentives to stimulate integration of recycling strategies in high added-value production chains close to locations where the waste is generated. This review offers a survey on techniques aimed at this purpose, particularly focused on the conversion of residues from different food sectors into bio(nano)materials.

1. Introduction

In the past century, the development of anthropic activities has resulted in a massive energy demand and consumption of resources which seriously impacted on Planet ecosystems and biodiversity, mostly through the release of wastes in the different environmental compartments including biota, air, water, land and aquatic sediments. The high rate of increase of the World population and the per capita needs have further accentuated the problem, making residues of industrial productions a global issue from both economic and ecologic/social standpoints because of disposal costs, hazard to human health, land use for storage, land and water pollution, climate change, etc. To cite only few numbers, more than 8 million tons of plastic are dumped each year into the oceans, and in 2017, an estimated 5 trillion of plastic pieces littered the seas.[1]

Pertinent to this context and strictly consequential to human activities is also the generation of biodegradable residues or bio-wastes (BW) whose nature, however, is not yet unambiguously defined. European Commission has proposed to include garden and park waste, food processing and kitchen waste from households, restaurants, caterers and retail premises, and food plants,[2] while on a more general basis, the literature expands the class of BW to domestic and sewage wastes, manure, food wastes and residues from forestry, agriculture and fisheries.[3] Whichever the classification, BW represent an enormous amount of organic and inorganic matter: the World Bank has estimated that by 2025, municipal solid wastes (only a part of BW) of the urban areas around the world might reach 2.2 billion tonnes per year, and waste generation rates might double over the next two decades in developing Countries.[4]

The most common disposal of biowastes is currently through the microbial decomposition under either aerobic or anaerobic conditions, thermal degradation and delivery in landfills. In recent years however, the potential of BW has received increasing attention by Academic

and Industrial communities aimed to identify strategies to convert low-valued wastes into new materials and products, and concurrently, developing technological and business models based on waste-to-value enterprises by the integration of biowastes processing within biorefinery schemes has been described.[5],[6] In this respect, fish/shrimp wastes, fly ashes, lignocellulosic food derived wastes, pig bristles, cattle manure and household wastes are becoming model examples of BW (Figure 1).

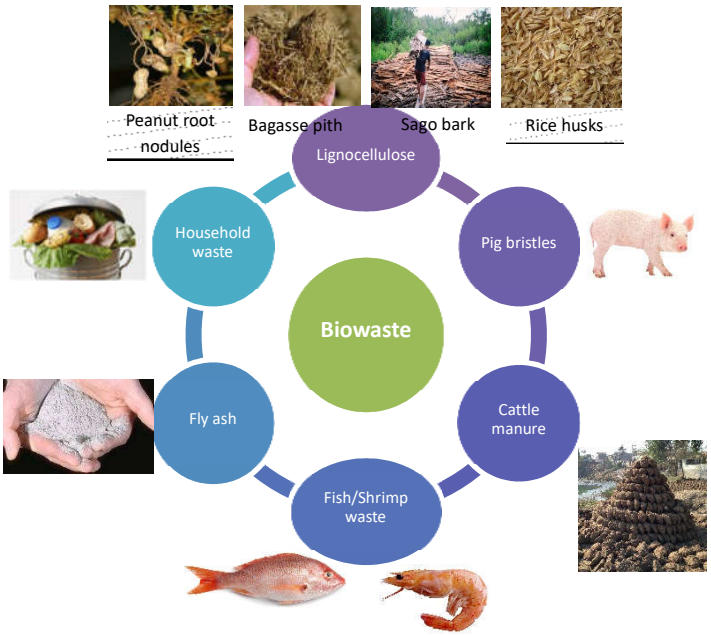

Figure 1. Most common biowastes

The vast generation, pervasive presence and chemical richness of such residues, are contributing to make their valorization one of the most promising perspectives for both an effective reduction of the environmental impact of BW and economic profit. The following section summarizes some properties and potential of these residues.

Fish/Shrimp waste (F/SW). The impressive growth of World per capita fish consumption from 12.6 kg in the early 1970s up to 19.8 kg in the early 2010s has pushed the United Nations' 2030 Agenda for Sustainable Development and FAO to recognize not only the primary role of fisheries and aquaculture for food security and nutrition, but also the needs to reduce fishing beyond biological sustainability, and improve the recovery and upgrading of wastes.[7,8] This is imperative to lower the impact of the anthropic exploitation of marine resources and preserve coastal environments. Recent estimates indicate that discards from the world's fisheries exceed 20 million tons per year that correspond approximately to 25% of the total production including by-catch ("non-target" species) and fish processing wastes.[9,10] Fish residues are comprised of whole waste fish, fish head, viscera, skin, bones, blood, frame liver, gonads, guts, some muscle tissue, etc. and represent a source of several potentially valuable molecules including oils, proteins, pigments, bioactive peptides, amino acids, collagen, chitin, gelatin, etc., [11] for the recovery/upgrading of which, many processes and technologies have been reported in the past decade or so.[12, 13] Yet, there is still way to go for large scale implementation. Of the major issues with F/SW, other than the unpleasant odor, the highly variable degradation times must be mentioned. Organic fish wastes rapidly decompose in hours or days according to environmental conditions, while exoskeletons of shrimps and crustaceans are extremely stable and recalcitrant to chemical or enzymatic

breakdown. This implies significant differences along the treatment/valorization chain of fish residues and side streams, dealing with their transport, storage and delivery to biorefining operations. The entity of this problem has been addressed through specific actions within Horizon 2020, the biggest EU research and innovation programme.[14]

Fly ash. Fly ash is traditionally defined as the main inorganic by-product from combustion of pulverized coal in power plants, comprised of a mixture of unburned carbon and inorganic oxides such as silica, lime, hematite, alumina, potassium oxide, magnesium oxide, and titania.[15] As such, fly ash from coal (CFA) is not a biowaste. However, in search for energy alternatives during the past fifteen years, several technologies have been developed based on co-firing biomass including residues of the forest industry and agricultural wastes from cereal production and oil extraction factories, with coal.[16,17,18] Mixtures of coal with up to 20 wt% of residual biomass have been used to the purpose, generating the so-called co-combustion fly ash (CCFA). This practice allows a more economical and environmentally friendly use of coal with reduced pollutant emissions.[19] Although biomass can also be combusted separately at power plants, two considerable challenges are the lower heating value and corrosivity (due to the salt content) of bio-residues. A technology to cope with these problems has been recently proposed by burning wood biomass (pellets, chips and sawdust) in the presence of low-alkali CFA (≤4 wt%).[20] The by-product of this combustion process has been referred to coal bio ash (CBA). Notably, it has been demonstrated that CBA is a better substitute for cement compared to CFA. Applications of fly ash have been extensively reviewed in recent years: favorable physicochemical characteristics such as sphericity of particles, porosity, light texture, low bulk density, and high surface area, account for the use of fly ash in a plethora of fields, as additives for construction and ceramic materials, catalysts, solids for soil and water remediation and recovery of precious metals, etc.[21,22] In this respect, technology transfer to biomass fly ash has been recommended not only for its potential in reducing CO_2 emission, but also for its benefits especially as an additive to increase in the porosity and lower the density microstructure of concretes.

Lignocellulose (LC). Lignocellulose is the most abundant renewable biomass on earth with an estimated global production of about 181.5 billion tonnes per year.[23] [4] Most of this material is involved in the natural carbon cycle of terrestrial ecosystems, undergoing microbial decompositions and transformations which ultimately afford CO_2 and water. However, a significant portion of LC generates biowastes, mostly coming from forestry and agricultural industries, which are promising sources for energy, chemicals, materials and food thanks to the content of phenolics, polysaccharides, and proteins.[24] Major challenges of lignocellulosic biorefineries (LCB) come from the strong interactions occurring between LC-components (cellulose, hemicellulose and lignin), which depend on the lignin content, crystallinity of cellulose, and particle size, and make this biomass a highly resistant and recalcitrant structure.[25] The key for success of LCBs largely relies on effective fractionation pre-treatments of feedstocks to separate LC-components and allow their further processing into biofuels and biochemicals. Of the multiple methods developed for the LC deconstruction, current technologies mostly exploit thermochemical conversion such as hydrothermal liquefaction, acid and alkaline hydrolysis, enzymatic hydrolysis, steam explosion, mechanical milling and ammonia fiber expansion; however, other less energy demanding procedures are emerging based on extrusion and dissolution in ionic liquid solvents.[21,26,27]

Pig bristles. In 2013 only, pork meat processing co-generated approximately 222 thousand tons of wet pig bristles and hooves in the EU, with disposal costs estimated slightly over four million Euros.[28] Although pig bristles particularly, consist for 90% or more of a valuable protein such as keratin, digestibility of this bio-waste is rather challenging because the protein is packed with fibres cross-linked by multiple disulfide bonds which confer exceptional stability towards common proteolytic enzymes such as trypsin, pepsin and papain.[29,30] Notably, a promising technology is currently being developed in the Danish project keratin2protein,[31] by which tailor-made microbial consortia cultivated in an industrial process are used for the degradation keratin into a protein enriched product which has been proposed as an alternative high-value feed for fish. This (sustainable) approach is under study to partly relief issues posed by the global demand of aquaculture feed that is estimated to reach 71 million t by 2020, almost doubled with respect to 2008, and ten-fold the request of 1995.[24,32]

Cattle manure and derived waste. Cattle manure has been used as a soil fertilizer for centuries, and this is still a living practice all over the world. Besides macro and micronutrients, manure also provides organic matter determinant for health of agricultural soils. FAO has recently reported that considering only the nitrogen (N) inputs, global manure production from all livestock increased 66%, from 73 to 124 million tonnes of N from 1961-2016, with manure applied to soils increasing from 18 to 28 million tonnes of N, and N input from manure left on pasture increasing from 48 to 86 million tonnes of N.[33] However, inappropriate manure management and excessive applications can also have detrimental effects on the environment, contributing to the contamination of water and soil resources and to increased greenhouse gas (GHG) emissions. A considerable interest has therefore developed towards anaerobic digestion (AD) of manure as an option to provide bio-methane for local energy needs in animal husbandry and farming.[34] Burning such bio-waste to generate power and CO_2 may become a climate-neutral practice, meaning that it does contribute mitigating the increase of GHG concentrations due to methane from unmanaged livestock residues.[35] It should be noted however, that the low carbon to nitrogen (C/N) ratio in animal manure brings about a moderate yield of biogas, which often does not justify capital costs for farm-scale plants. Effective solutions to improve the overall (gas) productivity have been conceived trough the introduction of carbon-rich co-substrates into the anaerobic digester.[36] Many examples have been reported of co-digestion of mixtures of manure with agro- and lignocellulosic- wastes and energy crops (maize, grass, wheat straw, palm pressed fiber, whole stillage from fermentative processes, corn stover, algae, etc.), food wastes, and even crude glycerol from the biodiesel manufacture.[35,37,38,39,40,41] Manure valorization has been explored also by other flexible technologies, in particular, hydrothermal liquefaction (HTL) to produce bio-oil (biocrude); regardless of initial composition of residues, the resulting liquid needed further upgrading processes before it could be used as a transportation fuel.[42,43]

Household waste. The World bank has estimated that in 2016, the release of solid household waste HW originated as discards from daily-life domestic activities in the worlds' cities, amounted to a footprint of 0.74 kilograms per person per day.[44] HW, also known as residential waste or domestic waste, has a highly heterogeneous composition including not only C-rich organic materials as food scraps, garden waste, paper mostly as cardboards and newspapers, and natural textiles, but also plastic and glass bottles and boxes, metals from cans, electronic waste (E-waste), etc. (Figure 2)

HW composition is influenced by factors such as culture, economic development, climate, and energy sources, which generally point out how urban waste streams are richer in organic

matter for low- and middle-income Countries, ranging from 40 to 85% of the total, while the release of paper, plastic, glass, and metal fractions increases for high-income Countries.[45] Table 1 illustrates three model case studies exemplifying the scenario.

Figure 2. Types of household wastes

Table 1. Composition of household waste in model urban areas

Entry	Urban area	HW composition (% of waste fractions)						Ref.
		Food	Plastics	Paper	glass	Metals	Misc.[c]	
1	Dehradun city, India	≥80	~7	~8[a]	~1[b]	na[d]	~4	46
2	Saudi Arabia, Coastal area	40-70	10-15	10-35	5-10	5-10	5-15	47
3	Scotland	23	32[e]	20	8	na[d]	17[f]	48

[a] Including cardboard. [b] Including ceramic scraps. [c] Miscellanea including cloths, silt, dirt, rubber. [d] Not available. [e] Including mostly healthcare waste, plastic films and dense plastics. [f] Including only garden waste.

The organic residues of HW, particularly food wastes make up the largest single waste type and often the most abundant fraction of the overall discards. Therefore, not surprisingly, research on HW-management strategies are frequently focused on the valorization of food wastes which belong to the general family of bio-wastes pertinent to the present paper.[49] This topic has been examined by some recent review papers that highlighted the following major aspects: [50,51,52] i) although a generally accepted definition of food waste is still missing and estimations on generated amounts are not yet consolidated, approximately 1.3 billion tons/year, i.e. one third of the food produced for human consumption, is wasted globally with contributions of 92.4, 90, 61, 6.2, 4, and 2 million tons/y from China, Europe, United States, South Korea, Australia, and Japan, respectively; ii) efforts are presently being addressed on the upgrading of food waste to biofuels and bio-products. In this respect, most promising technologies for bioenergy production are based on transesterification of oils and fats to produce biodiesel, fermentation of carbohydrates to bio-ethanol or bio-butanol, anaerobic digestion to bio-methane (see also previous paragraph), dark fermentation to produce hy-

drogen, pyrolysis and gasification to obtain oil and syngas, hydrothermal carbonization to get hydrochar; while, for the synthesis of bio-based molecules and materials, attention is focused on chemical, chemo-enzymatic, and biotechnological treatments of food waste to obtain mostly biomonomers for polylactates and polyhydroxyalkanotes, succinic acid, furfural and furans, and phenolic compounds; iii) cases study available so far highlight the potential of integrating sequential steps of food waste valorization within the biorefinery concept and application prospects are becoming increasingly close to realization as alternatives to the residue disposal of in landfills.

In light of the above analysis and pressing need to reduce worldwide production of biodegradable residues and improve their management, this contribution as a tutorial review aims to providing an insightful definition of the valorization concept of bio-waste.

2. Biowaste to biomaterials

Biomaterials are designed to engineering biomedical devices able to replace a part or a function in the human body. Due to their direct interaction with living organisms, biomaterials must combine stringent requisites of biocompatibility, pharmacological acceptability (non-toxicity, non-allergenicity, non-immunogenicity, etc.), mechanical strength, proper weight and density, and cost-effectiveness.[53,54] The synthesis of such materials from both natural sources and biowastes is therefore a challenging area that is currently being investigated through several approaches. This section will overview the preparation of some representative bio-waste derived materials.

2.1 Collagen and collagene-based biopolymers

Collagen is the most abundant fibrous protein found in the human and animal body.[55] Among 29 different structures of collagen that have been identified, the most common ones are type **I** present in bones, skin, dermis, vasculature, tendons, ligaments, cornea, and organs, type **II** constituting cartilages, type **III** found in reticular fibers of most tissues, spleen, skin, lungs, liver, type **IV** in basement membrane, forms basal lamina, and type **V**, which is associated with type **I** collagen, especially in the cornea. Collagen molecules are composed of three α-chains intertwined in the so-called collagen triple-helix (Figure 3).[56]

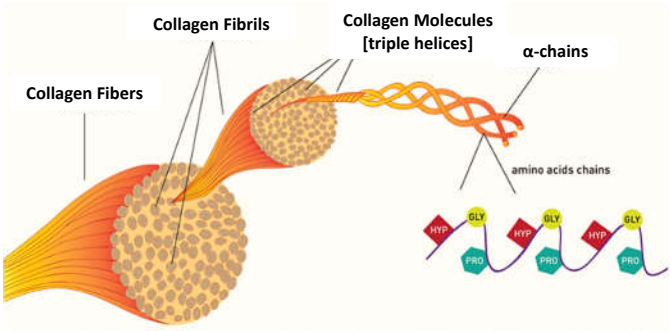

Figure 3. Collagen structure. Adapted with permission from http://blog.nkdnutrition.com/collagen-synthesis/.

The structure, mainly stabilized by intra- and inter-chain hydrogen bonding, is the product of an almost continuous repeating of the Gly-X-Y- sequence, where X and Y are often proline and hydroxyproline, respectively. The short N- and C-terminal regions, called telopeptides, do not form triple helical structures: these portions are comprised of 15-26 amino acid residues mostly of lysine, hydroxylysine, and their aldehyde derivatives, which undergo intra- and inter-molecular covalent

cross-links forming the basic unit of collagen fibrils. The typical strong nature of skins, tendons and bones is due to a network of cross-linked collagen fibrils.
Collagen exhibits remarkable bioactive properties, including biodegradability, non-immunogenicity, biocompatibility and low antigenicity which account for its extensive use as a biomaterial in a variety of applications in medical, cosmetic, tissue engineering, and food sectors (Figure 4).[57,58]

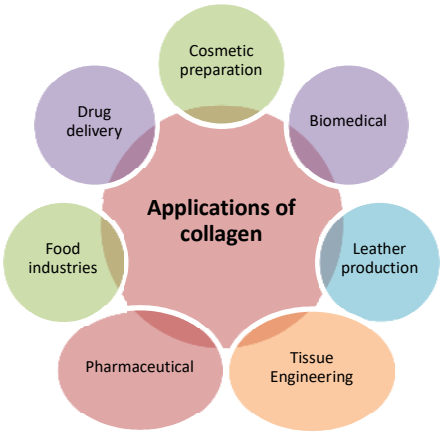

Figure 4. Applications of collagen

The different types of commercial collagens are obtained from a variety of animal connective tissues through extraction procedures based on acidic, alkaline, or neutral solubilization or enzymatic treatments. These processes, however, are rather expensive due to the moderate extraction yields and/or partial degradation of the product collagen. For example, enzymatic breakdown may cleave the terminal cross-linked portion of collagen, producing weak living tissue equivalents.[59] In search for methods improving yields and compositions, the use of biowastes, especially the organic fraction of fish discards (see above), has been explored as a low cost and ecofriendly source of collagen. First studies in this field date back to over 20 years ago,[60,61] but recent developments are attracting increasingly attention also for large scale productions. Among them, an interesting procedure has been designed starting from defatted samples of flatfish skin which were treated in acetic acid (0.05 M; 1:100, sample:acetic acid, w/v) and extracted by an industrial ultrasonicating equipment of 8 L operating at 20 kHz. After 4.5 h at 4 °C, collagen yield was up to 46%, twice higher than that achieved by conventional methods.[62] The extract was proved to be native type I collagen. Another successful protocol was implemented starting from sole fish skin using a response surface methodology (RSM) with Box-Behnken design (BBD).[63] The collagen yield was optimized up to a maximum of 19.27±0.05 mg/g of fish skin, obtained under specific conditions (0.54 M acetic acid, 1.90 M NaCl, 8.97 mL/g solvent/solid ratio and 36 h). SEM analysis proved that the extract was in the form of fibrils with irregular linkages, displaying large porosity suitable for the incorporation of chemicals and drugs (Figure 5).

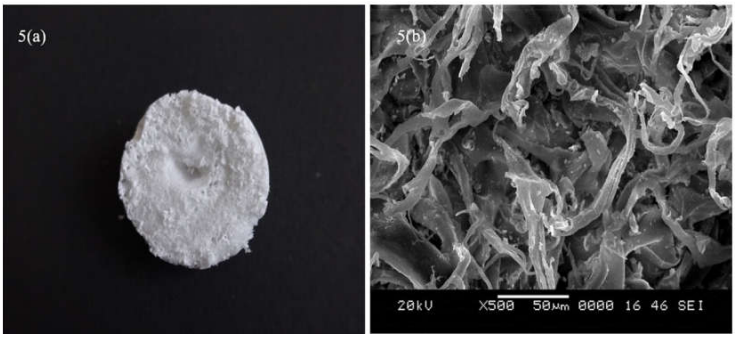

Figure 5. Lyophilised collagen from sole fish skin. (a) as viewed by the naked eye, and (b) SEM micrograph. Reproduced with permission from ref. 63

Collagen has been extracted also from waste fish scales using ionic liquids in which the activity coefficients (AC) of collagen were evaluated through a COSMO-RS computational approach.[64] The best solvent was identified as 1-ethyl-3-methylimidazolium acetate ([C_2C_1im][Ac]) for its low AC (inverse of solubility) and best fit sigma profile. After a pretreatment at 100 °C for 12 h, the extracted collagen was precipitated from the IL using a NaCl solution (2 M), and eventually collected in a yield of 3.1±0.5%.

Enzymatic digestion of fish residues was explored starting from aqueous suspensions comprised of defatted swim bladder wastes (of rohu, an Indian major carp), and a mixture of acetic acid containing pepsin [EC 3.4.23.1; 3000–3500 NF U mg^{-1}; solid:liquid ratio of 1:10 (w/v)]. Pepsin soluble collagen (PSC) was achieved with a yield of 465.2 g kg^{-1} (dry weight basis). The enzymatic breakdown was carried out at 4 °C for 48 h producing an extract that maintained the triple helical structure and exhibited a high fibril-forming ability.[65]

One last procedure mentioned here was devised through the application of a well-known technique in food industry, *i.e.* extrusion. An innovative extrusion-hydro-extraction (EHE) process was set up for the extraction of fish residues from tilapia fish scales (TFS).[66] The high heat (135 °C), high pressure, and high mechanical forces during the process acted synergistically to loosen chemical bonds between collagen and hydroxyapatite in fish scales, thereby providing type **I** collagens in yields up to 16 g protein/100 g crude protein content in TFS (dry basis). The method took advantage of typical benefits of the extrusion technique including continuous production, ease of operation, and little waste formation.

2.2 Chitin and chitosan derived biomaterials

Chitin and chitosan are natural aminopolysaccharides found together in nature.[67] The repeating units of chitin are comprised of β-(1-4)-2-acetamido-2-deoxy-β-d-glucose and β-(1-4)-2-deoxy-β-d-glucopyranose structures, respectively, producing a poly(β-(1-4)-N-acetyl-d-glucosamine, in a scaffold similar to that of cellulose (Figure 6).

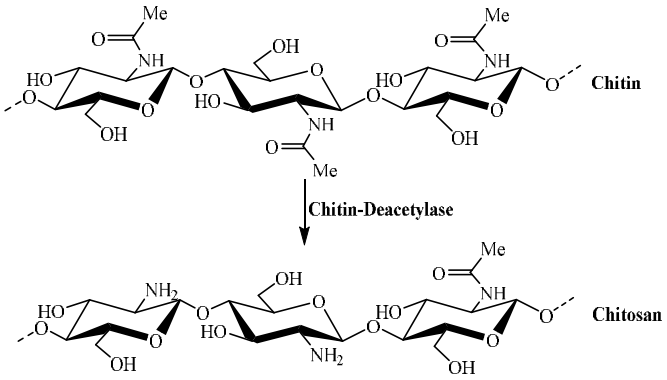

Figure 6. Partial deacetylation of chitin (top) for the formation of chitosan (bottom)

Indeed, chitin plays a role analogous to that of cellulose in plants, and collagen in the higher animals: it occurs as ordered crystalline microfibrils forming structural components in the exoskeleton of arthropods and crustaceans, and in the cell walls of fungi and yeasts.

On the other hand, chitosan is the N-deacetylated derivative of chitin: it is a copolymer composed of glucosamine and N-acetylglucosamine, with a degree of acetylation (fraction of N-acetylated glycosidic units) typically less than 0.35 (Figure 6). It has been demonstrated that chitosan produced by the enzymatic removal of acetyl groups from nascent chitin polymers has been implicated as an important component of the wall of fungal cells.[68]

Chitin. Commercial chitin is extracted from crustacean wastes of the fishing industry, the main sources being the shells of shrimp, crab, lobster, prawn and krill.[69] These bio-wastes usually contain chitin (20–30%), a protein portion (30–40%), inorganic salts mainly calcium carbonate and phosphate (30–50%), and lipids (0–14%). Therefore, isolation of chitin generally requires consecutive steps of deproteinization, demineralization, and discoloration during which removal of protein and inorganic components is followed by the elimination of colored pigments (astaxanthin, cantaxanthin, astacene, lutein and β-carotene) typically present in crustaceans shells.[70] The deproteinization is carried out either chemically with diluted aq. NaOH solutions (1–10%) at 65–100°C, or via biological fermentative treatments, while demineralization (removal of inorganic salts) takes place under diluted acid conditions with HCl, HNO_3, HCOOH, H_2SO_4, and CH_3COOH, and finally, discoloration is achieved at room temperature by solvent extraction mostly with acetone, ethanol, ethyl acetate or their mixtures. Crystalline chitin displays biocompatibility, biodegradability, antimicrobial activity, low immunogenicity, and eco-safety that makes it highly attractive in the field of biomaterials.[71] Although the extended hydrogen bonded structure of chitin limits its solubility in most solvents, and consequently, its processing, new applications of chitin have been described in recent years, especially for the fabrication of nanomaterials. One such example is the synthesis of multi-functional hybrid bio-aerogels based on cellulose nanofibers (CNFs) decorated with chitin nanocrystals (CNCs).[72] Once CNFs and CNCs were extracted from corn husks and shrimp shells, respectively, an environmentally friendly freeze-drying process was devised during which a mixture comprised of an aqueous solution of CNFs with dispersed CNCs was first frozen at -73 °C in a dry ice–isopropanol and then freeze dried in a lyophilizer at –88 °C under vacuum for 4 days. Figure 7a shows FESEM images of three CNFs aerogels with different amounts of CNCs (0, 1, and 2 % referred to as neat AR, AR1 and AR2, respectively).

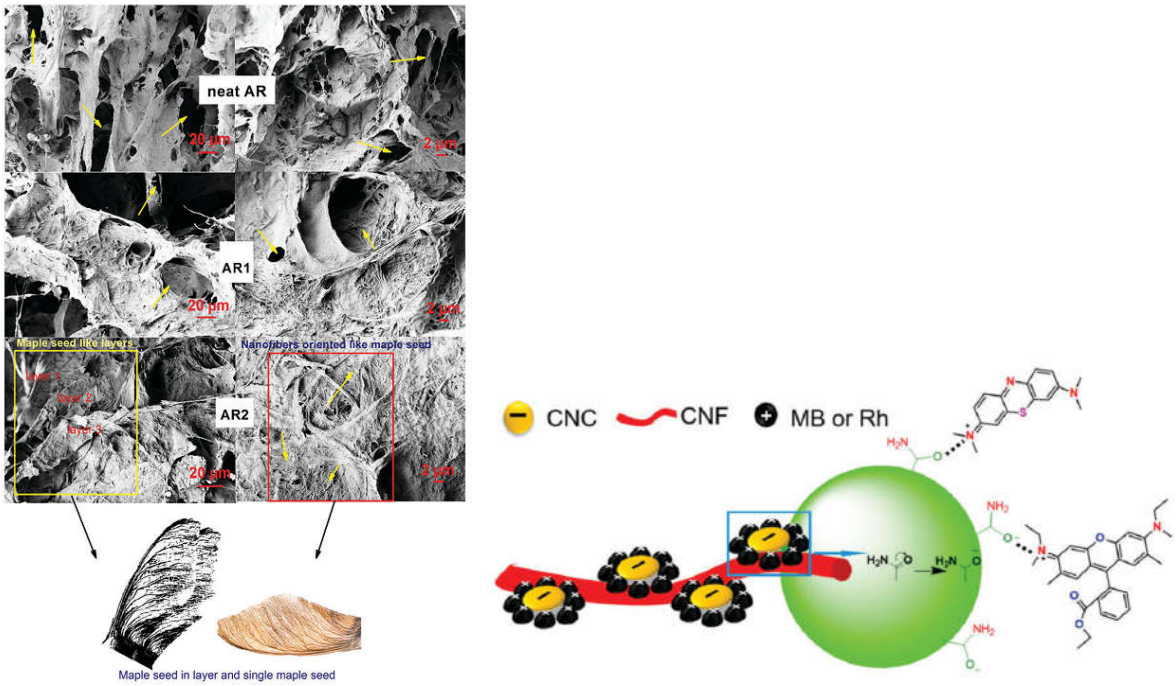

Figure 7. a) left: FESEM images of different aerogel; b) right: mechanism for adsorption of dyes (MB and Rh6G) into AR2 Reprinted with permission from ref. 72

Increasing the amount of CNCs modified the morphology of the material particularly in AR2 (bottom) whose fibers orientation mimicked the multi-layer maple seed structure. CNCs showed the tendency to locate in between the CNFs, reducing intermolecular interactions

between fibers. This was consistent with results obtained for removal of dyes (MB: methylene blue; Rh6G: rhodamine 6G) from aqueous solutions, which proved that AR2 was a far better adsorbent gel than neat AR and AR1. This behavior explained by the mechanism of Figure 7b, where interactions of positively charged dye molecules with acetamide-enriched AR2 favored adsorption (dotted lines). The multifunctional efficiency of AR2 was further confirmed by its superior antibacterial and antioxidant activity respect to neat AR and AR1.

A similar concept was applied through a different approach for the synthesis of a layer-by-layer spray coating of cationic CNF and anionic CNC suspensions onto poly(lactic acid) (PLA) films.[73] In this case, the attractive electrostatics between CNFs and CNCs promoted strong adsorption of thin alternating layers, while self-repulsion between CNFs or CNCs in any layer allowed each layer to pack more efficiently. The result was that films with at least two alternating coated layers, consisting of PLA-(CNC-CNF)n, showed significant reductions in O_2 permeability relative to PLA alone, even at elevated relative humidity (RH=70%). In terms of engineering applications, the potential of these films should be for a platform technology of 100% biorenewable barrier packaging, especially for foods, pharmaceuticals and electronics where oxygen permeability is a key problem.

Other remarkable uses of chitin have been reported for the fabrication of nanofibers with diameters less than 100 nm.[74] Upon dissolving chitin in HFIP (hexafluoro-2-propanol), such materials were prepared through different methods including self-assembly, microcontact printing, and electrospinning. Chitin nanofibers with high molecular weight were successfully electrospun using 1-ethyl-3-methylimidazolium acetate as an ionic liquid solvent. Major applications of the fibers have been described in tissue engineering mostly because of the structure similarity to glycosaminoglycans in the native extracellular matrix (ECM).

Finally, chemical modifications have been reported to convert chitin into several derivatives as for example, N- and O-sulfonated chitin relevant for the similarity to heparin (blood anticoagulant), dibutyryl- and carboxymethyl- chitin for biomedical applications in drug delivery.[75,76,77]

Chitosan. Chitosan is prepared by the deacetylation of chitin which involves the alkaline hydrolysis of the acetamide groups of chitin. Hydrolysis procedures have been reported under heterogenous conditions with a concentrated base (aq. NaOH, 40-50%; 100 °C) and inert atmosphere to limit depolymerization, or under homogeneous conditions, at 25–40 °C, by freezing–pumping-thawing (FPT) cycles of an alkaline aqueous suspension of chitin until dissolution. The latter (homogeneous) deacetylation reaction is a more effective process involving moderate alkali concentrations (≤13 wt%) and providing high-molecular weight chitosans with no chain compositional dispersion.[71]

A study examined the biological production of chitin achieved through lactic acid fermentation (LAF) of shrimp waste, and the subsequent deacetylation to chitosan.[78] Biological chitin (Bio-C) was obtained in a packed bed column reactor with maximal percentages of demineralization (D_{MIN}) and deproteinization (D_{PROT}) of 92 and 94%, respectively, after 96 h. The same shrimp waste was then subjected to acid/base chemical processing to get chemically extracted chitin (Ch-C). The comparison of the two methods proved that Bio-C had higher crystallinity index (I_{CR}) (86%) and M_w (1200 kDa) than the Ch-C. In the following step, the FPT deacetylation of Bio-C allowed to obtain chitosan with a mid-range M_w (400 kDa) and a degree of acetylation (DA) ca. 10% higher than that from Ch-C. The Bio-chitosan showed a block copolymer structure inherited from the parent crystalline Bio-chitin. Overall, the biological protocol combining LAF and FPT procedures was affective to avoid both loss of crystallinity and excessive depolymerization in the chitosan product.

Another effective method for the preparation of chitosan from shrimp shells started with usual deproteinization and demineralization processes followed by bleaching (discoloration) with ethanol. Thereafter, chitin was suspended in aq. NaOH (12.5 M), cooled down and kept frozen (24 h). The resulting chitosan obtained showed adequate physicochemical properties such as high solubility in acetic acid (1%), low ash content (0.063%), a molecular weight between 2.3 and 2.8 × 10^5 g/mole, a crystallinity index of around 40% and a deacetylation degree above 90%.[79]

Also, unconventional procedures for the deacetylation of chitin have been developed including thermomechanical processes, flash treatment under saturated steam, microwave dielectric heating, and intermittent water washings.[70] One such example was described for the preparation of low molecular weight chitosan (LMWC) through a solvent free, solid state mechanochemical method using chitin and crude shrimp shell powders.[80] In this approach, the simultaneous deacetylation and depolymerization of chitin was achieved in the presence of a base catalyst under mechanical milling conditions. In comparison to multi-steps procedures, this one-pot protocol showed advantages of increased efficiency, reduced environmental impact, reduced base consumption (to about 1/10), and narrow molecular weight distribution of the LMWC with a poly-dispersity value of only 1.1 (Figure 8).

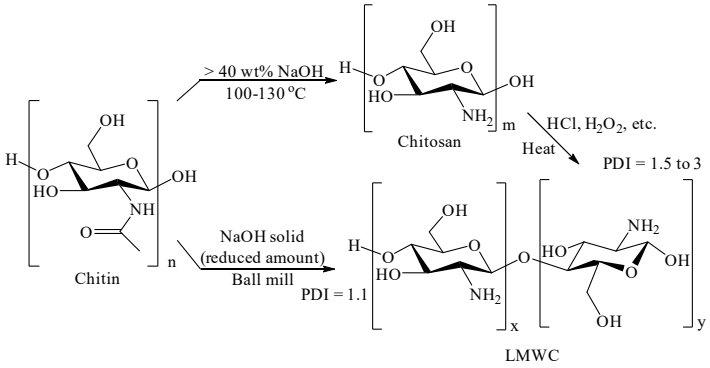

Figure 8. A two-step traditional method (top) is compared to and one-step mechanochemical procedure (bottom). The used commercial chitin had a low DD value of 3.5% and the DD values of chitosan-C and chitosan-H were around 80%. Adapted with permission from ref. 80.

Conversely from the parent chitin, chitosan is readily soluble in dilute acids due to easy protonation of free amino groups. The pKa (6.5) of these functions makes the polymer responsive to acid/base conditions, acting as a protonated cationic polysaccharide below physiological pH. Accordingly, chitosan is far more accessible than chitin for both chemical reactions and other uses.[70,81] Figure 9 summarizes the major fields of applications of chitosan.

Figure 9. Applications of chitosan.

Recently, antibacterial and antifungal activities of chitosan have been extensively reviewed, [69] concluding that several aspects may alter the behavior of the biopolymer. Chitosan is believed to act through electrostatic interactions between its positively charged protonated amino groups and the anionic components of the cell surface. Hence, the degree of deacetylation (and availability of free amino functions) as well as the derivatization at N and O atoms in glucosamine units are crucial to modify the hydrophilicity/hydrophobicity balance of chitosan. Increased antifungal activity were found for both highly deacetylated and for alkyl sulfonated chitosans, respectively. Quaternization reactions further improved the performance due to the permanent positive charge on N-atoms enhancing electrostatic interactions even at neutral pH. In addition, chitosans with a low molecular weight (LMW) in the range of 16-190 kDa, seemed most effective antifungals because they were likely to penetrate the cell wall more easily than mid- or high- molecular weight homologues.
Other recent papers have highlighted an increasing number of applications of chitosan derived from residual crustacean shells. Among strategies to modify and improve the surface characteristics of chitosan, graft copolymerization is an emerging technique, particularly the atom transfer radical polymerization (ATRP) for its compatibility with both aqueous and organic media and high tolerance toward a wide range of functional groups.[82] ATPR was used to graft chitosan beads with polyacrylamide or even more interestingly, to functionalize chitosan nanospheres (CTSNS) with poly(methylmethacrylate) (PMMA) and poly(methyl methacrylate)-b-poly(poly(ethylene glycol) methyl ether methacrylate) (PMMA-b-P (PEGMA)). The reaction produced individual nanospheres composed of a chitosan core and a densely grafted outer PMMA or PMMA-b-P (PEGMA) layer (Figure 10). Graft copolymers were potentially suitable for biomaterials.

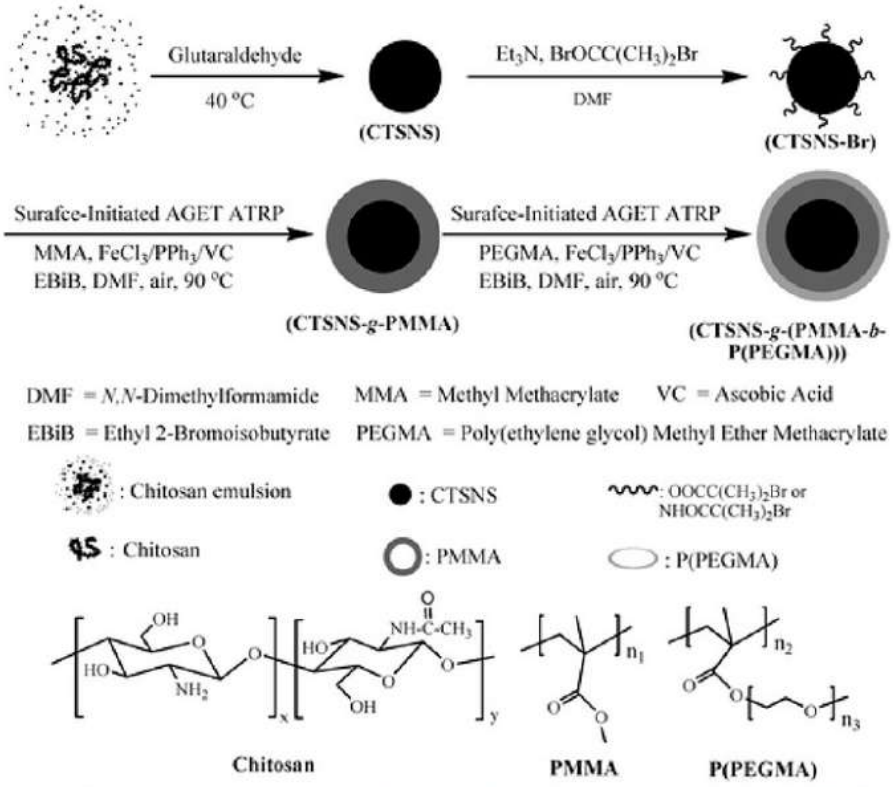

Figure 10. Surface modification of chitosan nanospheres (CTSNS) by ATRP for the synthesis of CTSNS-Br, CTSNS-g-PMMA, and CTSNS-g-(PMMA-b-P (PEGMA)). Adapted with permission from ref. 82

The interaction of chitosan with both synthetic and natural polymers has been described also in the formation of polyelectrolyte complexes (PEC) and layer-by-layer polyelectrolyte capsules or films.[83] In this case, electrostatic forces stabilize the final material: examples were reported in which chitosan was coupled to lipidic vesicles for bioadhesives and permeabilizers, or anionic alginate for protein release.
Chitosan and its derivatives have found applications as eco-friendly coagulants/flocculants to remove charged particles from wastewater.[84] Polyethylene glycol (PEG)-chitosan and polyvinyl alcohol (PVA)-chitosan composites were reported to adsorb aqueous nitrate ions with a capacity > 50.68 mg g^{-1}, while goethite/chitosan nanocomposite and carboxymethyl-chitosan were selective towards complexation of Pb (II), and Cd(II)/Cr(IV), respectively. Chitosan-based nanoparticles were also investigated to encapsulate and deliver bioactive compounds.[85] Prepared by either self-assembly and ionic gelation techniques, nanoliposomes derived from modified chitosan loaded with EGCG [(−)-Epigallocatechin gallate, the major bioactive compound in green tea] and catechin-loaded chitosan nanoparticles proved extremely efficient for slow and controlled release of encapsulated polyphenols in gastrointestinal tract. These studies are paving the way to exploit antioxidant, anticancer, and antibacterial properties of (tea) polyphenols through new biomaterials suitable for oral administration, with better stability and penetrating action in intestinal mucus, and intestinal epithelial cell targeting properties.

2.3 Hydroxyapatite

Hydroxyapatite (HA) of formula $Ca_{10}(PO_4)_6(OH)_2$ is one the most important material as a bone filler and scaffold for biomedical implants, not only because its chemical composition is similar to that of the mineral component of bone tissue, but also for bioactivity, biocompatibility, non-inflammatory behavior, high osteoconductive and/or osteo-inductive non-toxicity (Figure 11.[86]

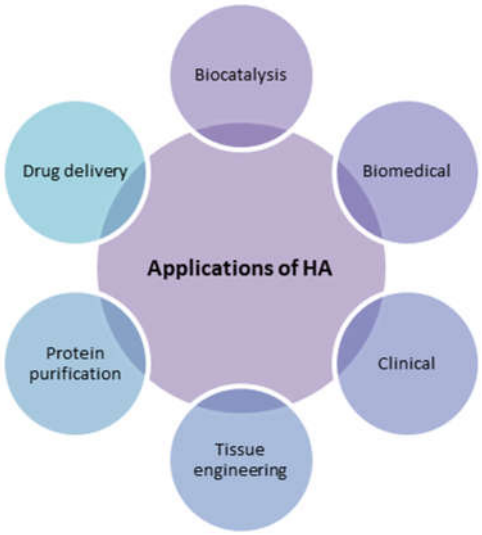

Figure 11. Major applications of HA

Although synthetic hydroxyapatite (sHA) can be obtained from commercial phosphate salts through precipitation, hydrolysis, hydrothermal (sol-gel), and microwave-based procedures,[87] a continuous effort is currently being made to valorise bioresources, and particularly biowastes, to extract natural hydroxyapatite (bio-HA). Consistently with the aim of this review, relevance is given here mostly to properties and applications and bio-HA. Extraction methods of bio-HA have been described starting from many different natural residues including animal bones, fish scales, eggshells, seashells and algae.[88] The treatment of animal bones either from bovine, swine or fish sources, generally requires removal of residual proteins through alkaline washing followed by high temperature calcination in the range of 600-1400 °C. In a comparative study, three protocols such as a thermal decomposition,

and subcritical water and alkaline hydrothermal processes were explored for the isolation of natural hydroxyapatite from bovine bones.[89] All methods afforded similar yields of bio-HA (~65%): though, thermal process (750 °C, 6 h) provided nanorod shaped HA of about 300 nm, while both alkaline hydrothermal process (NaOH, 25 wt.%; 250 °C, 5 h) and treatment in subcritical water (275 °C, 1h) gave pure hydroxyapatite nanoparticles of smaller size (<100 nm). In particular, subcritical water produced HA nanoflakes by plucking out residual collagen from bones.

Mild procedures were reported starting from fish scale (FS) waste for which simple deproteinization was carried out with HCl (0.1-1 M, rt), NaOH (5-50 wt%, 70-100 °C), and/or heating in boiling water, without any calcination at high temperature.[90,91] In a first example, bio-HA extracted from FS of *Tilapia nilotica* proved 4-fold more efficient than commercial hydroxyapatite for the selective adsorption and removal of Se (IV) in the purification of drinking water.[90] Even more remarkable were the properties of HA obtained from FS of golden carp (*Probarbus jullieni*): with respect to synthetic HA, bio-HA improved the formation of apatite during incubation in simulated body fluid, and it showed a higher osteoblast like cell adhesion on its surface, thereby proving its potential as a bioactive material for bone scaffold and tissue regeneration.[91] This behaviour was correlated to results of SEM, TEM, and EDX analyses showing that the bio-derived hydroxyapatite had a larger surface area, richer in Ca, and higher surface roughness than synthetic HA, and it was comprised of rod-shaped (50 nm in diameter) and flat-plate (ca. 20x100 nm, width x length) nanocrystals, respectively (Figure 12).

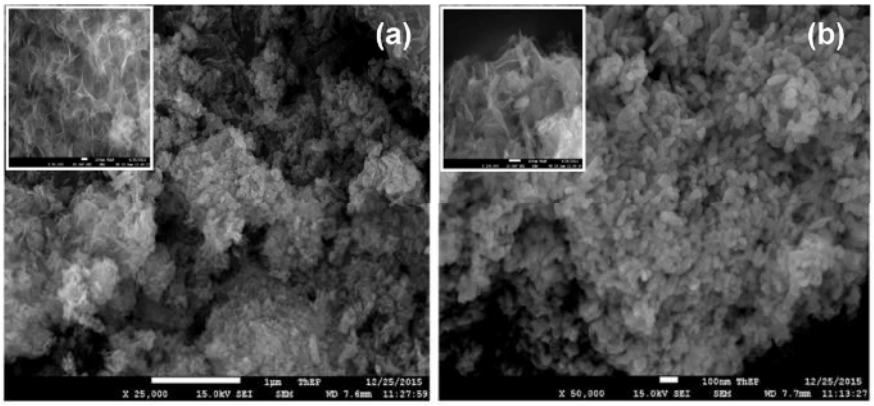

Figure 12. SEM images of bio-HA extracted from fish scale of golden carp (left) and synthetic HA (right). Reprinted with permission from ref. 91.

It should be noted here that sHA is a stoichiometric solid with Ca/P ratio of 1.67, while the bio-HA from bio-waste is not, due to the presence of trace amounts of cations and anions like Na^+, K^+, Mg^{2+}, Sr^{2+}, Zn^{2+}, and Al^{3+}, F^-, Cl^-, SO_4^{2-}, and CO_3^{2-}. This feature was reported to impart further beneficial properties to the bio-HA especially for the rapid regeneration of bone tissue.[88,92] In this respect, in vitro studies compared the biological response of sHA and three natural HAs extracted from fish bones of rainbow trout, cod and salmon, respectively, proving that bio-HA from trout and salmon showed a higher activity towards osteoblasts MC3T3-E1 than other tested materials. The result was ascribed to the effect of both CO_3^{2-} and Mg^{2+} ions (~0.7 wt%) able to stimulate cells proliferation, differentiation, adhesion, and formation of mineralized tissue.[93] A related concept was applied in the fabrication of a nanocomposite scaffold of natural hydroxyapatite and chitosan extracted from bovine cortical bone and shrimp shells, respectively, containing iron oxides nanoparticles of 10–40 nm.[94] This combination afforded a super-paramagnetic material with saturated magnetic intensity of approximately 3.04 emu/g and coercive force of 128.39 Oe, potentially suitable for bone healing therapies. Another interesting biocomposite was devised by the electrochemical deposition of a coating of chitosan, silver, and hydroxyapatite on anodized titanium substrate.[86] Although synthetic HA was used in this case, the synergistic effect of antibacterial properties of chitosan and silver ions

and biocompatibility of HA with bone tissue provided a coating preventing the risk of bacterial infection of implants.

Bio-wastes as eggshells and seashells has been also reported as a source for the preparation of HA.[88,95] In this case however, starting shell residues are calcined to obtain CaO which in turn, is converted to HA by reaction with phosphorous salts (Scheme 1). The final HA product is therefore a synthetic material.

$$CaCO_3 \xrightarrow{\text{calcination}} CaO + CO_2$$

$$3\ Ca_3(PO_4)_2 + CaO + H_2O \longrightarrow Ca_{10}(PO_4)_6(OH)_2 \qquad (a)$$

$$10\ CaO + K_2HPO_4 + 4H_2O \longrightarrow Ca_{10}(PO_4)_6(OH)_2 + 12\ KOH \qquad (b)$$

Scheme 1. Preparation of s-HA from CaO and two phosphorous salts (a and b).

2.4 Bioplastics

Bioplastics encompass both bio-based materials synthesized from biomass and bio-degradable plastics which break down into organic matter and gases mostly CO_2 by the action of naturally occurring microorganisms, such as bacteria, fungi, and algae. The latter may be of fossil or renewable origin.[96] Plastics can be therefore classified into four categories considering their biodegradability and raw materials (Figure 13).[97]

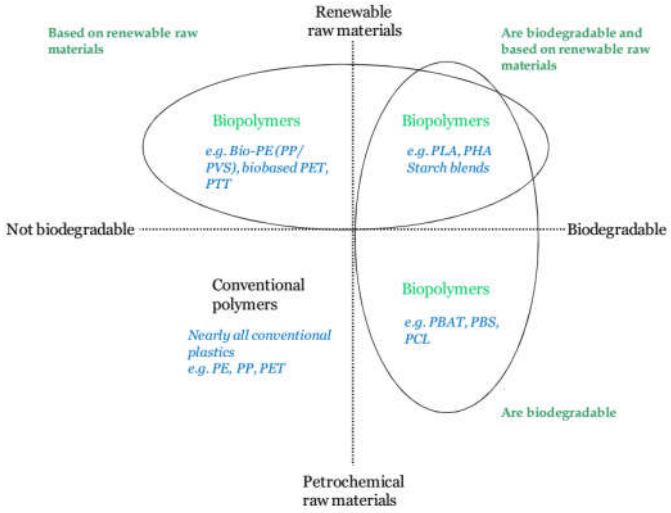

Figure 13. The four general types of plastics grouped by materials of renewable (top) and fossil (bottom) origin, not biodegradable (left) and bio-degradable (right) polymers, respectively.[97]

Examples of well-known non-biodegradable and biodegradable oil-based plastics include polyethylene (PE), polypropylene (PP), and poly(ethylene terephthalate) (PET) in the first group (non-biodeg.), and poly(e-caprolactone) (PCL), poly(butylene succinate/adipate) (PBS/A), and poly(butylene adipate-co-terephthalate) (PBA/T) in the second family, respectively.

On the other hand, not all bio-based plastics are necessarily biodegradable: contrarily to cellulose, cellulose acetate does not decompose in the environment. Likewise, bio-PET from bio-based ethylene glycol, whose content of renewable C is approximately 30 %, is not a biodegradable polymer.

European Bioplastics has estimated that the global production capacities for bioplastics is set to increase from around 2.05 million tonnes in 2017 to approximately 2.44 million tonnes in 2022, with fully bio-based and biodegradable biopolymers such as PLA (polylactic acid) and PHAs (polyhydroxyalkanoates) as the main drivers of this growth (Figure 14).[98] However, non-biodegradable polymers sourced from biomass as bio-PE (polyethylene) and bio-PET (polyethylene

terephthalate), which currently make up for around 56% (1.2 million tonnes) of the global bioplastics production, will follow different fates. The manufacture of bio-based PE is predicted to continue growing in the coming years, while that of bio-based PET will not at the expenses of a new 100% bio-based substitute as bio-PEF (polyethylene furanoate), with improved barrier and thermal properties for the packaging of drinks, food and non-food products.

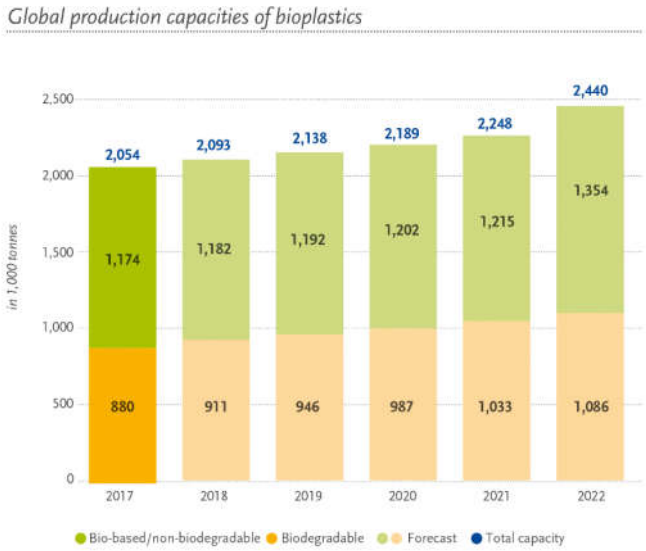

Figure 14. Trend in the global production of bioplastics.[98]

Due to the vast proportions and complexity of the subject related to bioplastics, this review paper will limit the analysis only to selected examples aimed to enable the Reader getting a perspective on innovative studies in the field of bioplastics prepared from secondary feedstocks as bio-wastes.[99] A recent investigation has proposed the use of myofibrillar proteins from residues of the processing of gilded catfish (*Brachyplatystoma rousseauxii*) to synthesize new plastic materials. Once extracted, proteins were mixed with aq. glycerol as a plasticizer and by a casting method, the resulting solutions were added to a silicone support and dried to get biofilms.[100] A response surface methodology was used to optimize the process design obtaining a bioplastic with 40% plasticizer (m/m) and 0.79% protein (m/v). The protein content imparted flexibility, resistance, low solubility and water vapor permeability which made the material suitable for food packaging. The good tensile strength (4.91 MPa) was ascribed to the extent of sulfhydryl groups at the myofibrillar protein surface which enabled the formation of covalent S-S in the biofilm framework. On the other hand, the hydrophilicity of fish muscle proteins due to their content of polar amino acids and hydroxyl (OH) groups was responsible for the low moisture barrier (water vapor permeability, WVP, in the range of 6-14 g m^{-1} s^{-1} Pa^{-1}) of the bioplastic.

A method for digesting edible vegetable wastes (rice hulls, cocoa pod husks, wastes of parsley and spinach stems) with trifluoroacetic acid (TFA) was explored to prepare amorphous cellulose-based plastics.[101] Dehydrated residues (3 wt%) were dispersed in TFA for variable periods (3-14 days) until dissolution; thereafter, casting processing and solvent removal under controlled humidity (60%) afforded biofilms (Figure 15). Interactions of TFA with cellulose component of the wastes brought about either breaking of the hydrogen bonds between neighboring cellulose chains (intersheet hydrogen bonds), and partial trifluoroacetylation of OH groups of cellulose with formation of amorphous materials. Mechanical properties of biofilms were largely dependent on the starting biowaste: residual silica in rice hulls derived material confer rigidity, while the triglycerides content in cocoa pod husks was responsible for the high stresses at break and strains of the corresponding film. This behavior along with the assessment of other properties (Young's modulus and interaction

with water) compared with common polymers (polypropylene, polyethylene, polyester) and elastomers (silicone and polyurethanes) indicated that vegetable waste bioplastics could open avenues for task-specific applications in packaging and biomedicine.

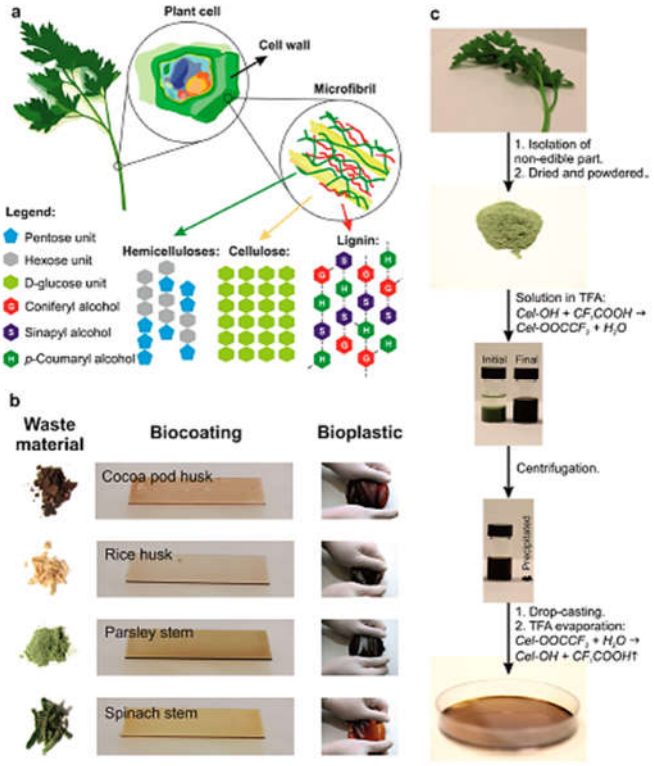

Figure 15. Edible plant waste products. (a) Schematic of the main components (hemicellulose, cellulose and lignin) of inedible plant wastes and their distribution at different scales. (b) Different edible plant wastes in diverse forms used in this study. Also, resultant biocoating and bioplastic products are shown. (c) Bioplastic production process from plant wastes to final films. Pulverized vegetable waste is dissolved in TFA after a proper aging time is reached the solution is cast into a Petri dish. Centrifugation can be used in order to eliminate undissolved parts. Adapted with permission from ref. 101.

On a further progress of this investigation micronized powders of vegetable waste from carrots, radicchio, parsley and cauliflower were dispersed in conc.d HCl (50 mg solid/mL) at 40 °C for 12 hours. Viscous dispersions were then dialyzed on a 3500 Da membrane against pure water and casted/dried to get the corresponding biofilms.[102] Confocal microscopy and SEM analyses proved the formation of homocomposites with particle sizes of 1-100 μm for carrots, parsley and cauliflower or larger for radicchio, displaying higher stiffness and lower ductility (Young's modulus and ultimate strength in the range of 0.2-1.3 GPa and 3-38 MPa, respectively) than bioplastics reported in Figure 15. Solid-state NMR characterization further showed that films were comprised of cellulose crystals fused together, with pectin and sugar portions acting as plasticizers. Notably, a blend polymer of polyvinyl alcohol PVA and carrot bioplastic showed an oxygen permeability (OP) of 31.2 cm^3 μm m^{-2} day^{-1} kPa^{-1}, lower than that of synthetic films, and migration of its components to food (tested against the dry food simulant Tenax®) well below 10 mg dm^{-2} which is the threshold value in EU for materials used in food contact. Similar low values of release to food, in the range of 1.2-3.5 mg dm^{-2}, were noticed also for bioplastic films as such. Overall, the new class of fully biodegradable compounds could be used for packaging or blended with other polymers for applications as disposable objects, cosmetics and biodegradable electronics.

Another frontier in this field is the preparation of biowaste-derived biodegradable plasticizers able to reduce brittleness, crystallinity, glass transition and melting temperatures, and improve flexibility and toughness of bioplastics.[103] Fully renewable plasticizers have been described for both poly(lactic

acid) and poly-3-hydroxybutiric acid (PHB). Significant examples are ethyl citrate synthesized by the esterification with bioethanol of citric acid (2-hydroxy-1,2,3-propanetricarboxylic acid) extracted from orange waste,[104] and tannic acid [1,2,3,4,6-penta-*O*-{3,4-dihydroxy-5-[(3,4,5-trihydroxy benzoyl)oxy]benzoyl}-D-glucopyranose] from residual lignocellulosic biomass.[105] It should be mentioned here that the use of bio-plasticizers is continuously expanding also for the replacement of conventional compounds in synthetic plastics. To cite only two cases, diesters of isosorbide, a common derivative of glucose, and highly branched polycaprolactone prepared by solvent-free copolymerization of ε-caprolactone and glycidol (a derivative of glycerol), have been recently proposed as effective plasticizers of PVC, one of the most valuable polymers worldwide.[106, 107] These bio-based plasticizers were claimed to improve thermal stability and stretchability (~20-fold higher) of PVC with respect to classical petro-based compounds as phthalate esters.

2.5 Silica and silicates

Biowastes are becoming increasingly interesting for the preparation of both silica and silicate salts. *Silica*. In the chemosphere, plants start the biogeochemical cycle of silicon with the uptake of silicic acid (H_4SiO_4) present in soil water. Silicic acid then undergoes polymerization and hydrated amorphous silica forms and accumulates in phytoliths that confer rigidity to plants.[108] Hydrated amorphous silica is naturally occurring in leaves, blades, husks, hulls, stems and roots of many terrestrial and marine plants, including rice, wheat, oats, horsetails, barley, grasses, and algae.[109] Among biowastes, one of the most silica-rich sources is rice husks (RHs) which are largely available, being typically 20−22 wt% of rice grains. The silica content amounts to ca. 20% of RHs dry weight which means that at the current rate of estimated global rice production of 500 Mt/y, perspectives for market applications of bio-silica and its derivatives are becoming attractive.[110,111] Approaches for the extraction of biogenic silica from RHs are mostly based on acidic pre-treatments for the removal of trace amounts of metals, followed by pyrolytic procedures carried out at variable temperatures and times usually in the range of 500-700 °C and 8-24 hours, respectively.[112] Conditions and process parameters (T and t) could be tailored to afford the synthesis of different added-value meso/macroporous silica. In this respect, one example described the pyrolysis of HCl-treated RHs at 700 °C for 2 h for the preparation of amorphous silica nanoparticles with narrow size distribution of 25−30 nm (Figure 16, left).[111] The so-obtained biogenic material was then suspended in aq. KNO_3 and subjected to a second pyrolytic cycle (800 °C, 2-8 h) to achieve a semicrystalline porous silica framework (Figure 16, right).

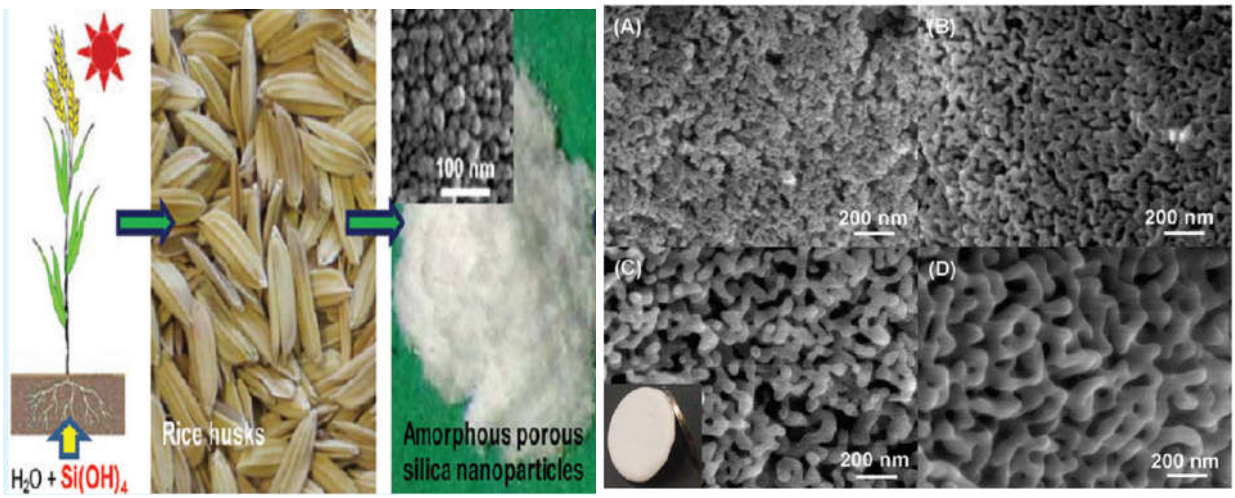

Figure 16. Left. Amorphous silica from rice husks. Right: modification of amorphous silica by aq. KNO_3. SEM images of meso/18icroporous silica frameworks: (A) 0.20 M KNO3, pyrolysis at 800 °C for 2 h; (B) 0.20 M KNO_3, pyrolysis at 800°C for 4 h; (C) 0.20 M KNO_3, pyrolysis at 800 °C for 8 h; (D) 0.50 M KNO_3, pyrolysis at 800 °C for 8 h. The inset in C shows a

coin shaped disk made of the corresponding semicrystalline porous silica framework. Reprinted with permission from ref. 111

As the pyrolysis was prolonged, K^+ cations progressively penetrated the silica structure thereby favoring the fusion of nanoparticles into a new well-defined porous material.

Another remarkable application of biogenic silica has been reported for the fabrication of nanomaterials used in lithium ion batteries. This subject was extensively reviewed in a recent paper describing protocols for the reduction of RHs-derived SiO_2 as such or in blend with carbon to obtain anodes of silicon or silicon/carbon (Si/C) composites and silicon carbide (SiC) materials, respectively.[113] Carbothermal reactions in electric arc furnace at 1700−2100 °C, and magnesio- and calcio- thermic reactions carried out with biogenic SiO_2 in presence of powdered Mg and Ca, respectively, at 650-720 °C, were used to prepare high purity silicon (99.9%). The potential of these procedures was discussed as a sustainable alternative for the conventional blast-furnace production of metallurgical-grade (MG) silicon by the reduction of quartz with charcoal at T>1900 °C.

A further contribution in this field proposed the extraction of SiO_2 from eco-friendly and inexpensive agricultural residues such as rice husk (RH), bamboo culm (BC) and sugarcane bagasse (SB) using a microwave assisted solid state ashing (MW-SS: 2.45 GHz; 650 °C for 30 min at 1200 W).[114] In the same work, biogenic amorphous silica was subjected to MW-mediated magnesiotermic reduction to prepare crystalline pristine Si that, contrarily to commercial Si nanopowders, displayed a coherent interconnected 3D porous with a wall thickness of∼23 nm and a pore diameter of 50−80 nm (Figure 17, top).

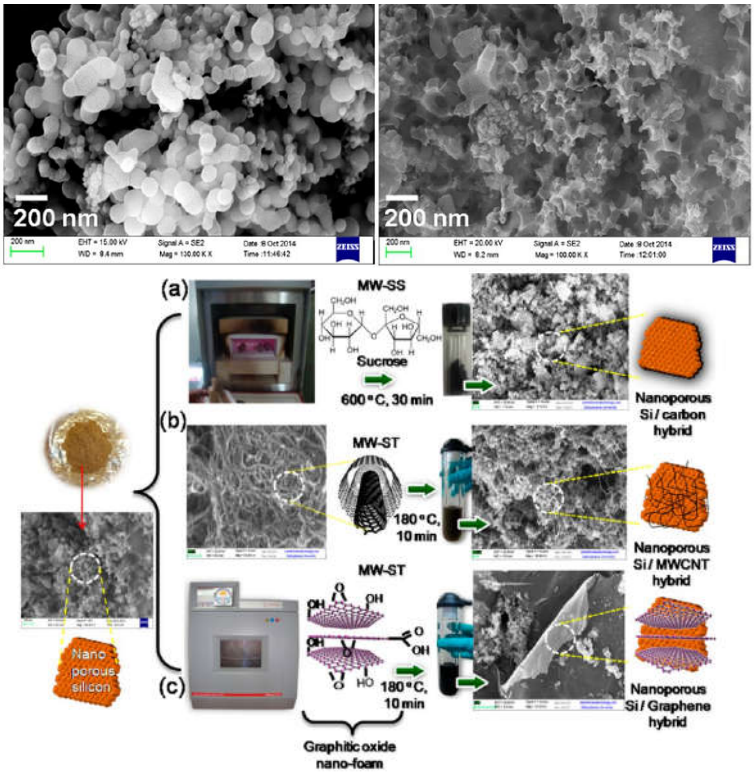

Figure 17. Top: Comparative FE-SEM images of commercially available agglomerated Si (left) and nanoporous Si obtained from biogenic silica via microwave assisted magnesiothermic reduction (MW-MR) within 30 min at 650°C (right). Bottom: silicon-based nanohybrid prepared by (a) microwave assisted solid state (MW-SS) decoration of carbon on 3D nanoporous silicon at 600 °C within 30 min, (b) microwave assisted solvothermal (MW-ST) synthesis of silicon and MWCNT nanonetworking at 180°C in 10 min, and (c) in situ one-pot MW-ST synthesis of 3D nanoporous silicon decorated on graphene nanosheets (GNS) at 180 °C in 10 min. Adapted with permission from ref. 114.

Cristalline Si derived from biogenic silica was finally decorated with dimensionally modulated carbon-based materials such as carbon(C), graphene nanosheets (GNS), and multiwall carbon nanotubes (MWCNT) (Figure 17, bottom). These materials offered delithiation capacities of 1997, 1290, and 1166 mAh g^{-1}, respectively, higher than pristine Si (956 mAh g^{-1}) from RHs, and interesting for next generation anodes in lithium batteries.

Silicates. Biogenic silicates can be obtained from biowastes via two general avenues including the chemical extraction of rice husks or the use of inorganic biowastes, mostly egg or oyster shells, as a source of Ca to provide the corresponding silicate salts.

Starting from RHs ash, chemical methods are generally based on alkaline extraction with aq. NaOH (1-3 M) under both conventional or microwave-induced heating.[112,113] Under these conditions, the silica content of ash is dissolved forming sodium silicate which is then neutralized to precipitate silica gels (Scheme 2).

$$\underset{\text{(ash)}}{SiO_2} + 2\,NaOH \longrightarrow Na_2SiO_3 + H_2O$$

$$Na_2SiO_3 + HX \xrightarrow[\text{Silica gel}]{} SiO_2 + NaX + H_2O$$

$X = Cl,\ NO_3$

Scheme 2. Chemical treatment of RHs ash

Starting from eggshells, a recent sol-gel combustion method was developed by first dissolving shells waste in nitric acid, and then adding magnesium nitrate, citric acid and TEOS (tetraethyl orthosilicate). Nitric acid served both to control the pH (=1) of the reaction mixture and to facilitate the hydrolysis of TEOS into silanol and ethyl alcohol. After 28 h at rt, poly-condensation of silanol and ethyl alcohol with citric acid provided a gel-like product which was finally decomposed in a muffle furnace at 400 °C. The synthesis yielded a nanocrystalline calcium magnesium silicate (akermanite, $Ca_2MgSi_2O_7$) with particle size in the range of 80–90 nm. In-vitro bioactivity tests of this material in simulated body fluid proved the formation of a crystallized hydroxyapatite layer on its surface, thereby disclosing its potential for applications in hard tissue regeneration.[115]

The synthesis of excellent adsorbents for environmental metal remediation was conceived starting from oyster shells (OS), an abundant biowaste products from mariculture. Calcium silicate hydrates (CSH) were first prepared through the calcination of OS in the presence of fumed silica at 650 °C for 2 h, followed by a hydrothermal treatment at 150 °C for 12 h. EDS, SEM and TEM analysis proved that CSH were a mixture of calcium silicate hydrates and calcium carbonate with a hierarchical porous structure of a large surface area comprised of thin nano-sheets each of which was assembled by nanofibers with width of around ten nanometers, and length of hundreds of nanometers. The surface of CSH was then modified by a multistep sequence including the functionalization with 3-aminopropyltriethoxysilane, and further reactions with glutaraldehyde and polyethyleneimine (PEI) (Figure 17).[116]

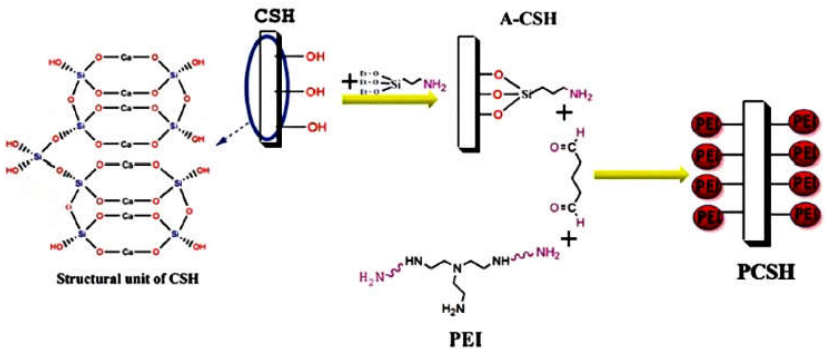

Figure 17. Synthesis of PEI-functionalized calcium silicate hydrates (PCSH).

Adapted with permission from ref. 115.

The grafting of PEI did not modify the size and morphology of the final material (PCSH) with respect to CSH; however, the high density of surface amino groups able to chelate metal cations strongly improved the adsorption capacity of PCSH up to 256 and 203 mg g^{-1} for aq. Cr(VI) and Cu(II), respectively. This (capacity) was much higher than that of CSH, OS and many other adsorbents in literature.

2.6 Additional examples

Besides the examples detailed in the above paragraphs of section 2, several other studies on the fabrication of biomaterials derived from biowastes have been described in the literature of the past fifteen years. Table 2 provides a summary of additional relevant examples.

Table 2. Biomaterials derived from biowastes

Entry	Biowaste	Prepared biomaterials	Ref.	Entry	Biowaste	Prepared biomaterials	Ref.
1	Bovine bones	Mineralized collagen	117	21	Fish waste	Gelatin	118
2	Silver carp skin	Collagen	119	22	Fish Fin & chicken feather waste	Protein	120
3	Mantis shrimp muscle	Collagen	121	23	Fish bone	Calcium phosphates	122
4	Puffer fish skin	Collagen	123	24	Groundnut & coconut shell, rice husk, palm fruit bunch and palm fruit stalk	Cellulosic fibers	124
5	Cuttlefish skin	Collagen	125	25	Pig bones & teeth	Hydroxyapatite	126
6	Brown backed toad-fish skin	Collagen	127	26	Eggshells	nanostructured hydroxyapatite	128
7	Fish (*Lates calca-rifer*) scales	Collagen sheet	129	27	Eggshells	Mesoporous hydroxyapatite NPs	130
8	*Loligo uyii* skin	Type V collagen	131	28	Fish scales	Hydroxyapatite Scaffolds	132
9	Eel fish skin	Type-I collagen	133	29	Shrimp shells	Bioplastic	134
10	Milkfish scales	Collagen	135	30	Chicken feathers	Bioplastic	136
11	Prawn shells	Chitosan	137	31	Fish scale	Bioplastics	138
12	*R. oryzae* fungi on potato peels	Chitosan	139	32	Rice husk	Polyester bioplastic	140
13	Goatskin	Collagen-chitosan biocomposites	141	33	Food industry	Bioplastic	142
14	Fish (*Labeo rohita)* scales	Chitin and chitosan	143	34	Fruit peel	Bioplastic	144
15	Shellfish	Chitosanases	145	35	Wood mill effluents	Bioplastic	146
16	Crustacean	Chitin	147	36	Rice husk	Porous SiO_2	148
17	Blue crab	Chitosan	149	37	Rice husk	Nano silica	150
18	Crab shells	Chitin and chitosan	151	38	Rice and coffee husks	Cellulose nanocrystals	152
19	Shrimp shells	Chitosan and chitooli-gosaccharides	153	39	Cotton linters and kraft pulp	Cellulose nanocrystals	154
20	Beetle *(Catharsius molossus)*	Chitosan	155	40	Croaker fish skin	Gelatin	156

3. C- based and hybrid C-based nanomaterials

3.1 Nano-carbons and nanocomposites

The nanocarbons family encompasses sp^2-bonded carbon materials with a variety of morphologies, including fullerenes, nanotubes and nanoscrolls, 2D-honeycomb arranged graphene, nanodiamonds and activated carbon nanoparticles and fibers (Figure 18, left).[157,158] Nanocarbons combine unique properties of high mechanical flexibility (in the case of carbon nanotubes and graphene), stability, ultra-high surface area, low toxicity, biocompatibility and tunable electrical, physical and chemical properties by covalent and non-covalent functionalizations, that have contributed to make them increasingly popular as new materials for: i) fillers in composites and hybrids, ii) chemical- and bio-sensing in medicine, iii) energy electrocatalysis and energy storing in the fabrication of

supercapacitor electrodes, iv) bioelectronics platforms, v) enhanced supports for precious metal-based catalysts, vi) plant growth promoters, etc. (Figure 18, right). [159,160,161,162]

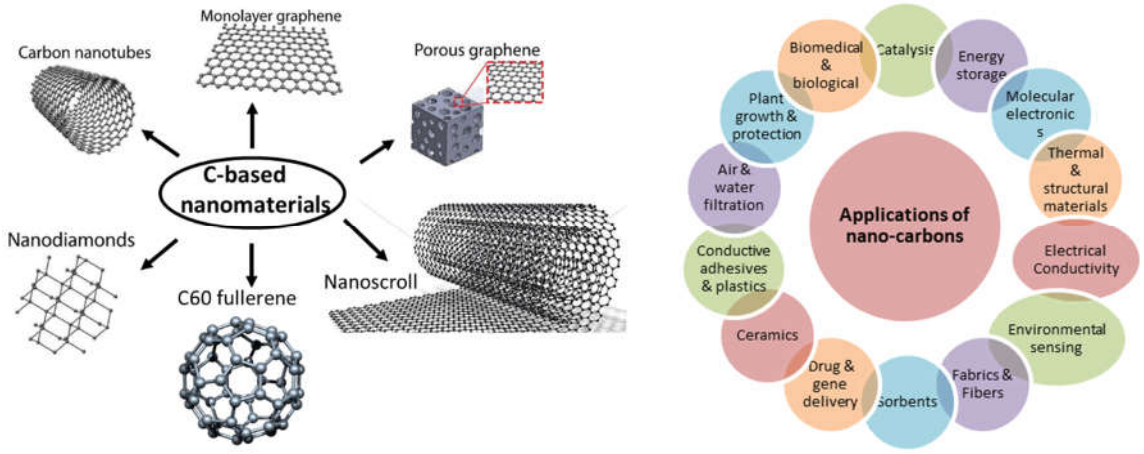

Figure 18. Left: examples of C-based nanomaterials; right: application fields of nanocarbons

In the recent past, the interest for nanocarbons has further expanded thanks to the implementation of sustainable synthetic routes starting from biowastes.[163] Collagen for example, turned out to be a promising source, especially that derived from discards of the leather industry. One of the first waste-to-wealth approach was described using waste goat skin trimming from which collagen was extracted and then treated by heating in a flow of Ar at 500-1000 °C.[164] Onion-like C-based structures, measuring up to ~20 nm, were obtained, each of them consisting of an assembly of defective spherical shells of graphite like layers separated from each other by approximately 3.363 Å. XPS and elemental analyses proved that the graphitic layers were doped by O- (6-15%) and N-atoms (3-15%) in the form of C=O and–O–C(O)O- groups, and N-bearing aromatic rings, respectively. These materials, particularly those obtained at 1000 °C, displayed an electrical conductivity of 4.6×10^{-1} S m^{-1} comparable to that of pristine graphene powder. In a second example, collagen extracted from raw cowhide trimming wastes, was added with aq. AcOH and superparamagnetic iron oxide nanoparticles (SPION). After gentle heating (40 °C, 12 h) and freeze-drying (4°C, 18 h), a sponge-like highly porous interconnected material was achieved in which the collagen fibrils were cross-linked with the inorganic nanoparticles (Figure 19, top).[165]

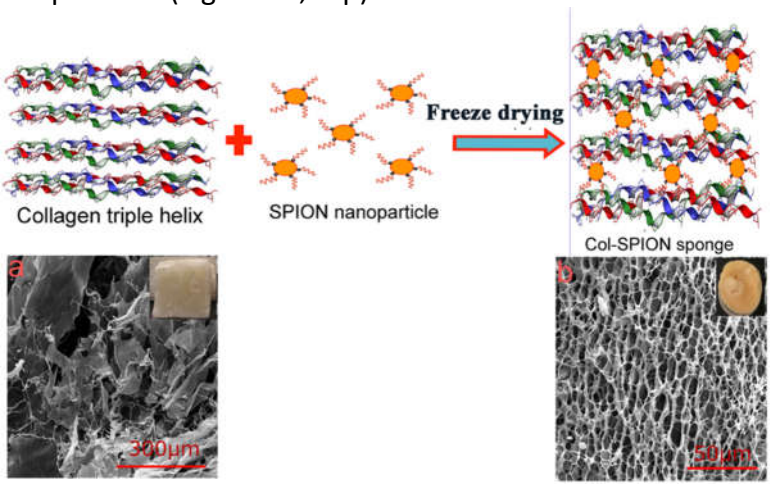

Figure 19. Top: Pictorial view of a hybrid composite sponge. Bottom: SEM images of (a) pristine collagen sponge and (b) Col-SPION hybrid sponge. **Adapted with permission from ref. 164**

Characterization of the composite proved that the inclusion of SPION into the organic matrix did not alter the triple helical structure of collagen, but strong interactions occurred between the two

components of the material explaining its remarkably different 3D morphology with respect to a pristine collagen sponge (Figure 19, bottom). The structure of the SPION-incorporated collagen sponge was responsible not only for an improved mechanical stability, but also for a good biocompatibility that was assayed in the proliferation of model cells (293T). The latter (biocompatibility) was ascribed to both the large porosity and the presence of iron nanoparticles which promoted cell adhesion and prevented the swelling of the composite. In a further development of this study, the same type of cowhide trimming waste derived collagen was added with aq. $FeCl_3$, freeze-dried, and finally heated at 1000 °C in an inert atmosphere. A hybrid bi-functional material comprised of iron nanoparticles encapsulated in nanostructured graphitic carbon was so fabricated with a surface area of 307.5 m^2/g, a conductivity of $3.64\pm0.13x10^{-3}$ S/cm, and a saturation magnetization of 12.3 emu g^{-1}.[166] The adsorption capability of the carbon shell and the separation of electron-holes by iron nanoparticles, made the material an efficient photocatalyst for environmental remediation applications and a potential new system for anodes in Li ion batteries with a reversible capacity of 384 mAh/g, higher than that of graphitic carbon or graphene nanosheets. In this field, another approach was conceived starting from untreated softwood sawdust which was soaked with aq. iron nitrate and carbonized at 800 °C in a muffle furnace under a flow of N_2.[167] Catalytic iron carbide nanoparticles (Fe_3C) were thermally generated *in situ*. These etched through the biomass producing straight and bamboo-like intertwined tubules (diameter of 20–50 nm) with walls comprised of graphitic layers similar to multi-walled carbon nanotubes. The same carbothermal reduction was carried out by premixing $Fe(NO_3)_3{\cdot}9H_2O$ with either $Ca(NO_3)_2{\cdot}4H_2O$ or $Mg(NO_3)_2{\cdot}6H_2O$, to prepare nanocomposites of Fe_3C/graphite combined with nanoparticles of metal oxides such as CaO or MgO, respectively. All such materials were of interest for range of technologies such as battery electrodes, electrocatalysts and water treatment.

The synthesis of a hybrid material comprised of copper sulfide (Cu_2S) carbon nanocomposite was reported starting from an unprecedented approach for the valorization of pig bristles (pb) as a biowaste acting as a source of both C and S. Under microwave irradiation, a mixture of pb, ethylene glycol, and copper chloride underwent a thermo-degradation reaction by which disulfide bonds of keratine, the protein constituting pb, broke down releasing sulphur in the form of ions which in turn, combined with Cu^+ and self-aggregated C-particles. The properties of chalcocite, Cu_2S, as a p-type semiconductor (band gap of 1.2 eV) were exploited for the catalytic photodegradation of methyl red, a model for environmentally recalcitrant organic dyes.[168]

Bio-waste oil palm leaves (OPL) have been described as another source for the preparation of porous carbon nanoparticles (PCNs), through pyrolytic treatments carried out at 500-700 °C under a nitrogen atmosphere.[169,170] Naturally occurring silica in starting leaves acted as a template to provide carbon nanospheres with particle sizes in the range of 20-85 nm. Silica was then removed by alkaline washing (NaOH,2.5 M, rt). Voltammetry studies proved that PCNs-based electrodes had a specific capacitance as high as 368 F/g at 0.06 A/g in 5M KOH, indicating that PCNs could be effective precursors for the fabrication of supercapacitors electrodes.

3.2 Carbon dots

Carbon dots, usually abbreviated as CNDs (carbon nanodots) or C-dots, are nano-sized (<10 nm) quasi-spherical carbon particles containing a carbon core functionalized with some of the most common groups, primarily carbonyl and hydroxyl moieties. As such, C-dots are a class of carbonaceous nanomaterials distinct from fullerenes, graphenes, carbon nanotubes, and other carbon allotropes.[171] After their fortuitous discovery in 2004, C-dots have rapidly emerged as a new class of versatile materials able to integrate optical properties of quantum dots based on semiconductors with electronic properties of carbon materials.[172] C-dots have been and are

therefore extensively investigated for applications in biosensing, bioimaging, drug delivery, photocatalysis, photovoltaic devices, and optoelectronics.

The two most used methods for the synthesis of C-dots is the top-down approach in which large macroscale carbon sources are broken down by arc-discharge, laser ablation, and electrochemical reactions, and the bottom-up approach in which thermal, hydrothermal, and microwave-assisted routes allow to assemble C-dots from molecular precursors. This synthetic flexibility allows to modify the degree of carbonization, size, and morphology of C-dots, though issues related to batch-to-batch reproducibility, control of surface properties, purification, and characterization may represent a limit for the application of these materials.[173] In this respect, the use of natural products including biowastes as starting materials for the preparation of C-dots has been reviewed in two recent papers.[174,175] The subject is still in its infancy and there is much room for further discovery, but some original strategies are emerging. For example, hydrothermal-assisted methods have proved effective for a variety of biowastes such as fruit peels, fish scales and rice husks. The heating of an aqueous dispersion of pomelo peel wastes at 200 °C for 3 h was reported to produce stable dispersions of C-dots of 2-4 nm, which upon excitation at 365 nm, showed a PL emission peak at 444 nm and an intense blue color under UV light (6.9% quantum yield) (Figure 20).[176]

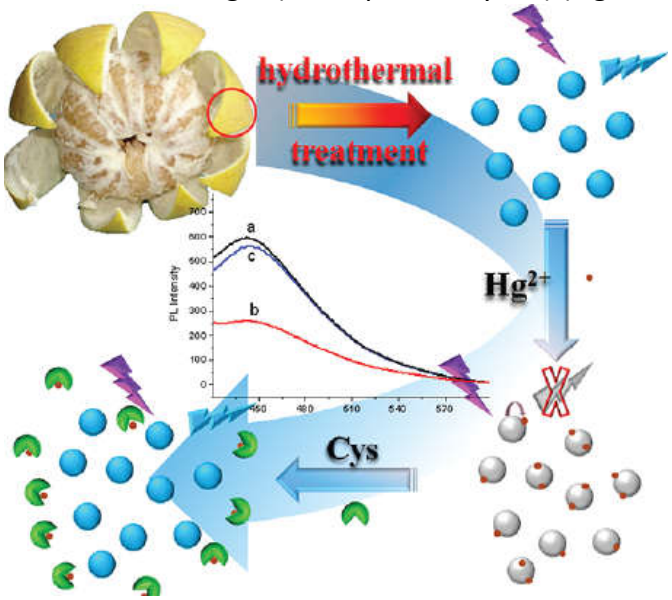

Figure 20. Hydrothermal treatment of pomelo peel for the synthesis of fluorescent CPs sensitive for the detection of Hg^{2+} ions. Adapted with permission from ref. 175.

Such carbon dots were effective as a sensing probe for label-free, sensitive detection of aq. Hg^{2+} ions with a detection limit as low as 0.23 nM. A similar approach was used starting from orange pericarp wastes which afforded C-dots with an average particle size of 2.9 nm, and PL quantum yield of 2.88%. The narrow size distribution suggested potential applications in nano-biotechnology.[177]

Another method for the preparation of *N*-doped photoluminescent C-dots was described using fish scales wastes of grass carp that were suspended in deionized water and heated at 200 °C for 24 h in an autoclave.[178] The generated C-dots were homogeneously sized particles of 2 nm with a remarkably high N-content of 14.6% (by XPS) (Figure 21). When excited at 365 nm, a broad emission peak at 430 nm was observed with a quantum yield of 17.08% due to the fluorescence enhancement effect of nitrogen doping. The PL effect was so strong that even at a very low concentration, aq. dispersion of C-dots gave very bright violet-blue luminescence (top inset of Figure 21). Notably, the fluorescence could be selectively quenched by the addition of ClO^- (up to 10 mM), making the fish scale derived C-dots a sensing system for this anionic species.

A multistep “bottom-up” synthesis of C-dots was described starting for rice husks (RHs). The non-oxidative thermal treatment of RHs (700 °C, 2h) initially generated an ash (RHA) containing both carbon and silica, which was further heated at 900 °C with excess NaOH to produce submicron-sized carbon flakes (RHCs) of 300-500 nm and sodium silicate. The latter was separated via aqueous washing and filtration. Solid RHCs were oxidized under acid/basic conditions and hydrothermally cut at 200 °C, to afford RH-C-dots of 3-6 nm (ca. 2 wt % yield based on dry RHs). Aqueous dispersions of such dots were highly stable and showed blue luminescence with emission in the range of 360-440 nm, upon UV excitation at 365 nm. Hela cell viability test confirmed that C-dots were biocompatible and useful for cell imaging via translocation into the cytoplasm. On the other hand, the recovered sodium silicate was used to synthesize mesoporous silica nanoparticles with a specific surface area of 466.3 m^2/g, and a pore diameter of 3.8 nm. The overall strategy offered an effective approach for a comprehensive utilization of RH biomass.[179]

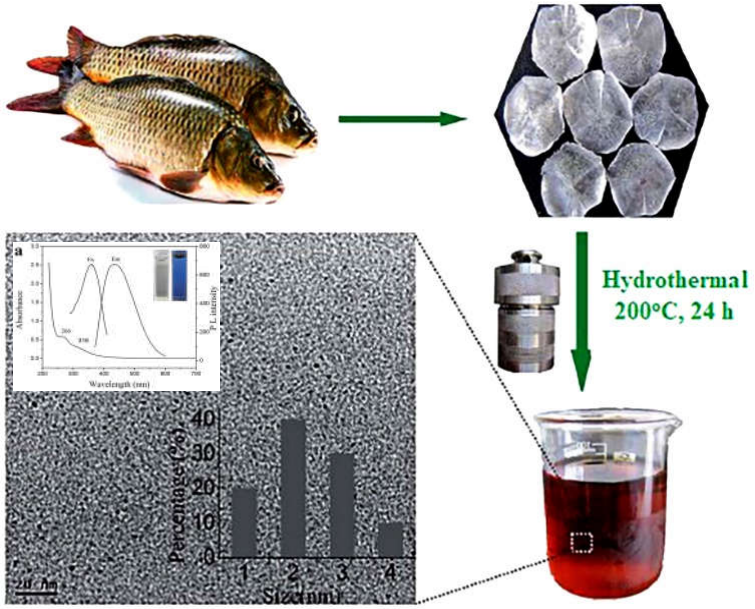

Figure 21. Schematic illustration of the formation of C-dots from hydrothermal treatment of fish scales. In the TEM image, insets show the particle size distribution histogram of C-dots (bottom) and their UV-vis absorption, excitation and emission spectra (top). Adapted with permission from ref. 177.

A microwave-assisted hydrothermal procedure has been also described for the fabrication of C-dots from biowaste, specifically in the treatment of an aqueous mixture of goose feathers, a major discard of the poultry industry, at 180 °C in a microwave autoclave (2 kW). After membrane dialysis (Mw=3500) against Milli-Q water, an aq. suspension of C-dots was obtained. C-dots displayed a uniform two-dimensional (2D) morphology with a diameter of 21.5 nm and a height of 4.5 nm, and a content (by XPS) of C, N, S and O of 48.4, 16.3, 1.9, and 33.3 wt%, respectively. Due to heteroatom-doping in the form of surface hydroxyl, carbonyl, carboxylic or amide groups, C-dots showed a high QY of 17.1% upon excitation at 340 nm and acted as selective photoluminescent probes for Fe^{3+} ions with a detection limit of 196 nM.[180]

A different synthetic approach was proposed by using strong acids as oxidants of biomass waste. Starting from dead neem leaves, pyrolysis in a split-tube furnace at 1000 °C (5 h, Ar) provided a fine carbon powder which was added to a 3:1 acid mixture of H_2SO_4 and HNO_3, and heated at 90 °C. After filtration (0.2 µm) and neutralization, a stable aq. dispersion of graphene carbon dots (GC-dots) was prepared. GC-dots were then subjected to a hydrothermal reaction in ammonia solution (30%) at 200 °C for 12 h, to obtain amino-functionalized dots (Am-GC-dots).[181] Some properties and

the optical behavior of these materials are summarized in Figure 22. The surface –COOH functional groups of GC-dots were responsible for the formation of a superlattice due to an extended H-bonding network in which nonradiative recombination of electron hole pairs was preferred in the intrinsic states. The corresponding green luminescence was attributed to surface energy traps. By contrast, surface $NH_3^+OH^-$ ion pairs led to single monodispersed particles in Am-GC-dots and suppressed the nonradiative path. The observed blue emission was ascribed to zig zag sites.

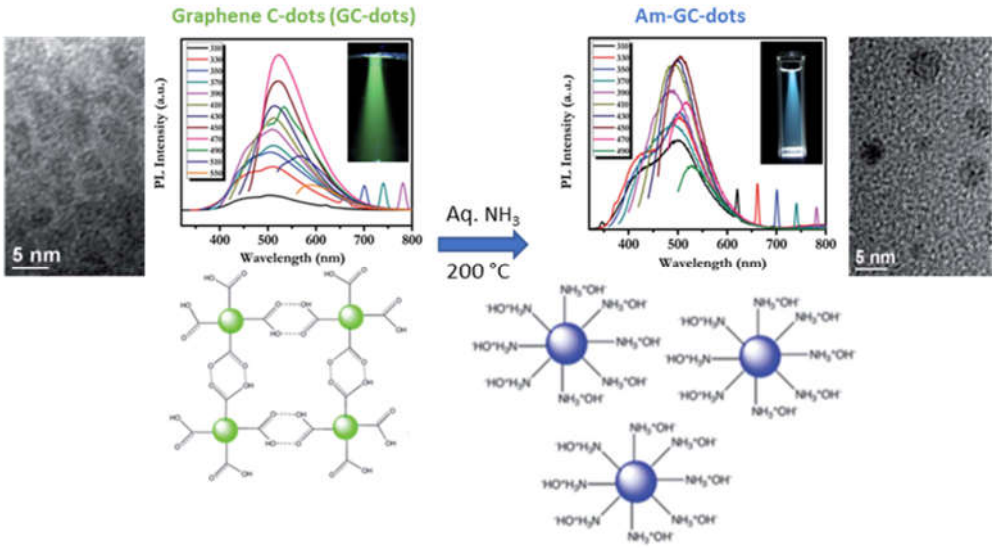

Figure 22. Top: HRTEM and PL data of GC-dots and Am-GC-dots at different excitations (left and right, respectively; Bottom: pictorial views of the GC-dots superlattice due to intermolecular H-bonding, and separated Am-GC-dots. Adapted with permission from ref. 181

Overall, Am-GC-dots showed not only much higher water dispersity and photoluminescence intensity than GC-dots, but they also exhibited selective photoluminescence "on–off–on" performance towards aq. Ag^+ ions.

3.3 Three-dimensional porous carbon nano-networks (3DCNT)

3D porous carbon nano-networks generally identify C-based materials with peculiar architectures comprised of loose three-dimensional network structures possessing a large number of meso- and micro-pores.[182] Biowastes have been recently proposed as starting materials for the fabrication of such structures. For example, a two-step pyrolytic treatment of goldfish (*carassus auratus*) scale waste carried out at 350-900 °C, was reported for the synthesis of N-doped hierarchically porous 3DCNT materials.[183] The thermal decomposition took place in the presence of $ZnCl_2$ that acted as a promoter for the dehydroxylation of fish scale, thereby increasing the formation of micro/meso-pores within the structure. Moreover, pyridinic- and graphitic-nitrogen dopant species (3-10 wt%) were key components to impart the materials with an electrocatalytic activity for oxygen reduction comparable to that of the commercial 20 wt% Pt/C catalyst in both alkaline and acid solutions (Figure 23).

In a different approach, a common biowaste as chicken egg shells membrane (ESM) was used for the preparation of both the electrode material and the bio-separator used in an asymmetric supercapacitor. The protein-rich ESM was firstly carbonized at 800 °C to obtain a 3D carbon network that retained the same fibrous structure of the parent ESM with macropores of 1-10 µm and fibers of diameter of 1-4 µm. Thereafter, the 3DCNT was chemically activated with KOH at 700 °C to form a sheet-like graphitic nanostructure with many surface micropores, which was finally utilized as a support to grow MnO_2 nanoparticles. The asymmetric supercapacitor was then assembled using

ESM carbon as the negative electrode, MnO_2 nanoparticle/chemical activated ESM carbon as the positive electrode, and natural ESM as the separator (Figure 24). This device displayed a high energy density of 14 W h kg^{-1} along with a power density of 150 W kg^{-1}. Significantly, the natural ESM based bio-separator displayed an impressive ion conductivity and cycling stability.[184]

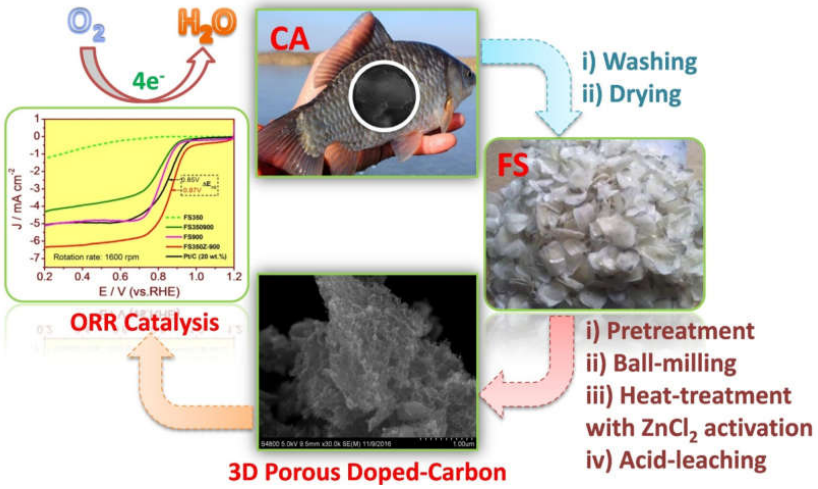

Figure 23. Synthesis of 3D-network nitrogen-doped porous carbon derived from protein-containing FS waste with $ZnCl_2$ activation. Adapted with permission from ref. 183.

Figure 24. Fabrication of an asymmetric supercapacitor using biowastes-derived materials from chicken egg shells. Adapted with permission from ref. 184.

In a further development of this study, another biowaste as ground cherry calyces (GCCs) possessing a 3D porous microstructure based on thin-sheets and microtubes, was selected as a starting material. The carbonization at 700 °C (4 h, under Ar) of GCCs did not induce a major structural fragmentation. However, the chemical activation/etching of the resulting carbon powder with KOH followed by a further pyrolytic treatment, provided a 3D scaffolding framework of porous carbon nanosheets (PCNS) with a typical hierarchical porous structure containing macroporous and mesoporous regions, and co-doped with O and N atoms. SEM analyses are shown in Figure 25 (a-c). TEM and XPS proved that the average thickness of the nanosheets was ca 10 nm (Figure 25 d), and the (atomic) contents of C, O, and N of PNCS were ~90.1, ~8.8, and ~1.1 %, respectively. The combination of macro-, meso- and micropores, the degree of graphitization, and the appropriate N, O-doping made this material suitable to fabricate electrodes for a high-performance supercapacitor displaying specific capacitance of 350 F g^{-1} at a current density of 0.1 A g^{-1} using 6 M KOH as electrolyte.[185]

Corncob sponge (CS) was proposed as another biowaste for the preparation of electrode materials. In the reported procedure, CS was mixed with KOH, and activated at 850 °C to obtain a nanocarbon material (ACS) which was doped with N and S by a second pyrolytic treatment (800 °C) in the presence of thiourea (Figure 26). The resulting N,S-ACS product showed a three-dimensional

interconnected honeycomb-like porous structure with a high accessible surface area (1874 m^2 g^{-1}) appropriate for a large ion storage and a rapid ion transfer. The total N and S contents were 5.11 and 2.86% distributed as pyridinic-N (35%), pyrrolic-N (17%), quaternary-N (29%), and pyridine-N-oxide (19%), and C-S-C and C-SO-C bonding, respectively.

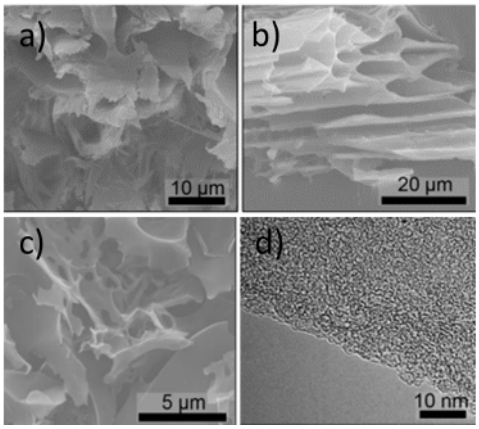

Figure 25. SEM images of: a) dry GCC; b) carbonized GCC; c) PCNS. TEM micrograph of PCNS (d). Adapted with permission from ref. 185.

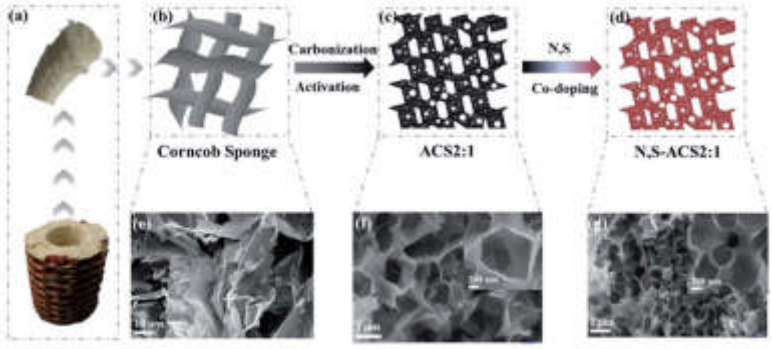

Figure 26. Fabrication procedures of N,S-ACS materials (top) and the corresponding SEM images (bottom). Adapted with permission from ref. 186.

Dopant elements induced structural defects increasing open channels and active sites and enhanced electron transfer (mostly N), and provided a high surface electron density (mostly S). Overall, an electrode fabricated with N,S-ACS delivered a specific capacitance of 404 F g^{-1} at 0.1 A g^{-1} and when assembled in a symmetric flexible solid state supercapacitor, the device offered an energy density of 30 W h kg^{-1} and a power density of 8000 W kg^{-1} (99% capacitance retention after 10000 cycles in a PVA/KOH gel electrolyte). This performance was promising for commercial applications in large scale energy storage.[186] Another material for supercapacitor electrodes was achieved starting from waste cotton seed husk (CSH). Pyrolysis/activation of CHS powder at 600-800 °C in the presence of KOH provided a 3D honeycomb-like porous carbon (a-CSH) with interconnected hierarchical (micro, meso-, and macro-) porosity and a high specific surface area of 1694.1 m^2/g. Moreover, a-CSH was nitrogen self-doped (2.62 at%). A symmetric supercapacitor assembled with an a-CSH-based electrode displayed a high specific capacitance of 52 F/g at 0.5 A/g, with an energy density of 10.4 Wh/kg at 300 W/kg (91% capacitance retention after 5000 cycles at 10 A/g).[187]

3.4 Additional examples

Besides the examples detailed in the above paragraphs of section 3, several other studies on the fabrication of biowaste-derived nanocarbon materials have been described in the recent literature. Table 3 provides a summary of additional relevant examples.

Table 3. Biowaste-derived nanocarbon materials

Entry	Biowaste	Prepared nanomaterials	Ref.
1	Sugarcane bagasse pith	Nano-porous activated carbon	188
4	Sago bark	Carbon nanospheres	189
5	Chicken eggshell	Nitrogen-doped fluorescent carbon nanodots	190
6	Coffee grounds	Hierarchically Porous Carbon Nanosheets	191
7	Wood wool	Carbon nano-onions	192
8	Mangosteen peel	Three-dimensional porous carbon	193
9	Rice husk	Carbon nanoparticles	194
10	Amazonian fruits	Activated nanocarbons	195
11	Tea plants	Carbon nanostructures	196
12	*Moringa oleifera* fruit shell extract	Ag-reduced graphene oxide nanocomposite	197
13	Paper pulping	Lignin-based carbon/ZnO nanocomposite	198
14	Pine cone	Pine cone-iron oxide nanocomposites	199
15	Eggshell	Pd/eggshell nanocomposite	200
16	Porcine bone	SnO_2/porcine bone	201

4. Metal nanoparticles (M-NPs) in colloidal dispersions

The small size of metal nanoparticles (M-NPs) in the range of 1-100 nm, most often below 10 nm, is responsible for an extraordinarily high surface area to volume ratio and large surface energy which explain the capability of M-NPs of adsorbing, capturing and recognizing small molecules at their solid surface. Due to these size- and shape- dependent properties, M-NPs have become increasingly popular in the past twenty years for a variety of applications including biosensing, catalysis, optics, antimicrobial activity, fabrication of computer components, electrometers, etc.[202] The large surface energy however is also the reason for the spontaneous tendency of M-NPs to coalesce into thermodynamically favored bulk (large) particles having less surface atoms with unsaturated bonds. The agglomeration phenomenon is ruled by the Ostwald ripening mechanism through which smaller particles release surface atoms able to diffuse in the solution and to stick to larger particles thereby lowering the total energy of the system.[203] To prevent this, electrostatic, steric and even the combination of these two, named as electrosteric, stabilization modes have been described to provide the spatial confinement of M-NPS by using polymers, surfactants, ionic liquids, solid supports, and ligands with suitable functional groups.[204] Another emerging approach involves protocols based on the use of biomolecules such as proteins/enzymes, flavonoids, polysaccharides, alkaloids, polyphenols, and vitamins, that are present in plant extracts and microbial cells, and may act as both bio-reductants and stabilizers for M-NPs (Figure 27).[205,206,207]

With respect to conventional chemical procedures, advantages of such biosynthetic methods include an improved eco-friendly profile because hazardous reductants and solvents (as, for example, hydrazine hydrate, sodium borohydride, and DMF) are avoided, and the production of non-chemically contaminated M-NPs which is relevant to minimize toxicity issues in biomedical applications. In this respect, biowastes are also receiving increasing attention. One of the first examples reported the use of polyphenol-rich red grape pomace as a reducing and a capping agent, to fabricate nanoparticles of Au, Ag, Pd, and Pt in aqueous media. In a typical procedure, a solution of selected metal precursors ($HAuCl_4$, $AgNO_3$, Na_2PdCl_4, and $HPtCl_4$) was added to a pomace extract and microwave heated at 52-55 °C (50 W) for 60 s. Crystalline nanoparticles of Au, Ag, Pd, and Pt

were obtained with size around 30, 10, 5-10, and 3-4 nm, respectively and variable yields of 80-90%.[208]

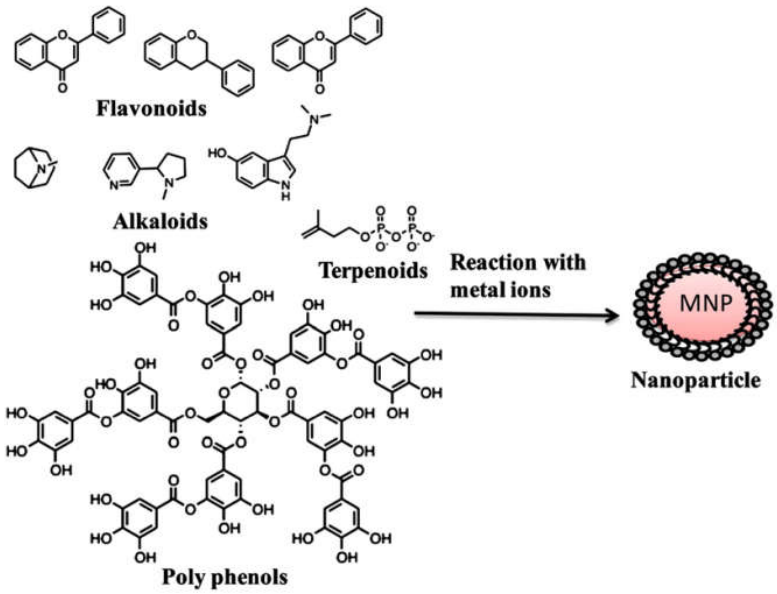

Figure 27. Common biomolecules in plant extracts for the synthesis/stabilization of M-NPs. Reprinted with permission from ref. 205.

A similar approach was used for the bio-reduction of aq. $AgNO_3$ in the presence of mango seed aqueous extracts. The formation of predominantly spherical and hexagonal Ag-NPs of ca 14 nm in size, was complete in 30 min at room temperature. In view of exploring the potential for biomedical uses, aq. mixtures of Ag-NPs and bovine serum albumin (BSA) were examined by fluorescence spectroscopy. The occurrence of a strong interaction between the protein and the metal particles with formation of a ground state complex, explained the remarkable quenching observed in the fluorescence of BSA.[209]

Another strategy was conceived starting from a protein-rich membrane (ESM) extracted by mild acid treatments of chicken egg shells. At ambient conditions, the reaction of ESM with aq. $HAuCl_4$ (0.1 mM - 0.1 M) afforded fluorescent Au nanoparticles stabilized either as a colloidal aq. solution or by adsorption on the membrane. It was hypothesized that amino, carboxyl and carbonyl functionalities constituting the structures of bacteriolytic enzymes (lysozyme and N-acetyl glucosaminidase) of the shell membrane, acted both as chelating and reducing agents promoting the conversion of aq. Au^{3+} to Au(0) in the NPs. Microstructural (TEM and SEM) and optical investigations proved the formation of particles below 20 nm in the form of pseudo- spheres and triangular prisms (Figure 28), that displayed intense red and blue emissions at around 630 ± 5 nm and 437 ± 5 nm, respectively, suitable for biolabeling and bioimaging applications.[210]

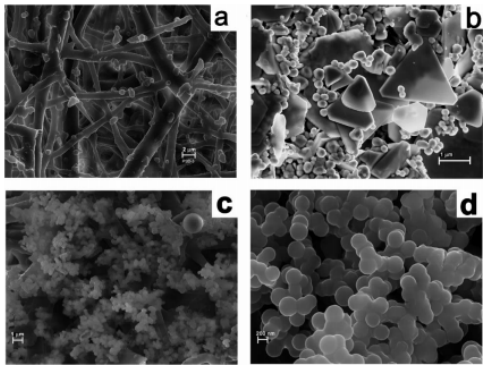

Figure 28. FESEM pictures of (a) bare ESM, (b) Au impregnated ESM and (c) and (d) 80 °C dried membrane showing spherical particles. Adapted with permission from ref. 210.

4.1 Solid supported M-NPs and metal nanocomposites.

The stabilization of M-NPs has been conceived through impregnation on solid supports and synthesis of nanocomposites which not only prevent the agglomeration of particles, but offer materials that can be more efficiently handled, *e.g.* for separation from reaction medium in catalysis and/or water disinfection. On this subject, the use of biowastes has inspired different approaches.

One such procedures started from a dispersion of an aqueous solution of $AgNO_3$, ammonia, and glucose dispersed in a mixture of rice husks (RHs) and rice husks ash (RHA). Under alkaline conditions, both deprotonation of silanol groups in RH/RHA and the formation the silver-ammonia complex, $Ag(NH_3)_2^+$ took place, thereby favoring the adsorption of Ag^+ on the support (Scheme 3, top). The glucose-mediated reduction of metal cations finally provided Ag-NPs of diameters ranging from 10 to 35 nm, impregnated on RHs/RHA (atomic silver % in the range of 0.23-0.77) (Scheme 3, bottom).

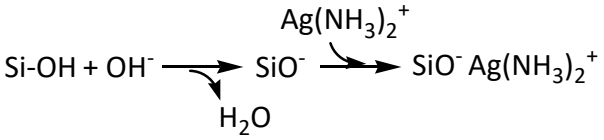

$$2\ OH^- + 2\ [Ag(NH_3)_2^+] + C_6H_{12}O_6 \rightarrow 2\ Ag^0 + 4\ NH_3 + H_2O + C_6H_{12}O_7$$

Scheme 3. Adsorption/reduction of Ag+ during the impregnation of Ag-NPs on RH/RHA.

Ag-NPs on RHs/RHA displayed a strong bactericidal effect for both Gram negative *(E. coli*) and Gram positive (*S. aureus*) bacteria, though metal leaching was detected.[211] Rice husk was also used as a starting material for a multistep synthesis of Au-NPs. Furnace calcination at 700 °C of HCl-treated RHs provided silica NPs of ca. 60-70 nm, which were functionalized by (3-aminopropyl)-triethoxysilane (APTES). The so-prepared amino-capped silica NPs favored the grafting of aq. $AuCl_4^-$ anions which were reduced by $NaBH_4$, yielding Au-NPs (ca. 2-4 nm) immobilized on the silica surface. The overall strategy is shown in Figure 29. Au-NPs on RH-derived silica exhibited excellent catalytic performance for the hydrogenation of 4-nitrophenol to 4-aminophenol, with no loss of activity after three recycles.[212]

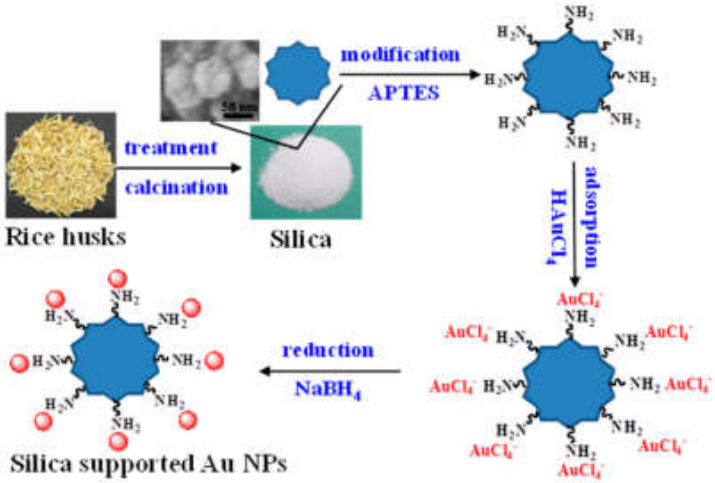

Figure 29. Preparation of RH-silica-Au NPs. Adapted with permission from ref. 212.

A versatile approach for the preparation of lignin-supported NPs of precious metals including Au, Pd, Ru and Re was proposed introducing a bottom-up mechanochemical methodology by which a solid mixture of a metal precursor and powdered Kraft lignin were ball-milled in steel milling jar. Although the reaction mechanism was not elucidated, mechanical breakdown of lignin plausibly brought about the formation of easily oxidizable (poly)phenolic species which could act as metal

reductants. Notably, the incorporation of NPs within lignin was dependent on the nature of the metal precursor with best results achieved with $HAuCl_4$, $Pd(AcO)_2$ and $Pd(acac)_2$, Ru(III) acetate, and $Re(CO)_5Br$, respectively. The corresponding M-NPs were highly monodispersed with size in the range of 3-6 nm, except for larger Au-NPs of ca 14 nm.[213]

A green synthetic procedure for the fabrication of metal-based nanocomposites was reported by combining the reducing/stabilizing properties of aqueous extracts from leaves of *Orchis mascula L.* to the use of a cheap support derived from a largely available biowaste as chicken egg shells. In a typical reaction, a suspension of powdered egg shells, a metal precursor as $CuCl_2{\cdot}2H_2O$, $FeCl_3{\cdot}6H_2O$ or their mixture, and an aqueous plant extract was heated at 70 °C for 3 h. Thereafter, Cu/eggshell, Fe_3O_4/eggshell and Cu/Fe_3O_4/eggshell nanocomposites were recovered by filtration. RP-HPLC-DAD analyses proved that the used aqueous extracts were rich of phenolic and flavonoid compounds (up to 2500–3300 GAE/dried weight of myricetin, caffeic and chlorogenic acids, luteolin 3-O-glycoside, kaempferol 7-O-glycoside, etc.) acting as bio-reductants according to the hypothesis of Scheme 4.

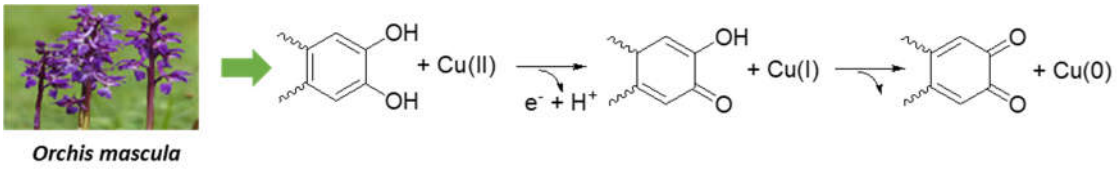

Scheme 4. The bio-reduction of Cu(II) mediated by a polyphenol from *Orchis Mascula* extract

EDX and TEM characterization confirmed that metal amounts and NPs sizes were 11.05, 24.69, and 9.80+46.32wt% and 5, 8 and 17 nm for Cu, Fe_3O_4, and Cu/Fe_3O_4, respectively. At ambient conditions, all nanocomposites proved effective catalysts for the reduction of a variety of contaminant dyes as methyl orange, congo red, methylene blue and Rhodamine B.[214] In a similar approach, an aqueous extract of *Myrica gale* L., a flowering plant of the *Myricaceae* family, was used as a reducing and stabilizing agent for the preparation of Ag-NPs immobilized on a powdered cow bone as a support. SEM and TEM micrographs of the Ag/bone nanocomposite showed that spherical metal NPs of 5–10 nm were distributed on the bone surface (Figure 30).

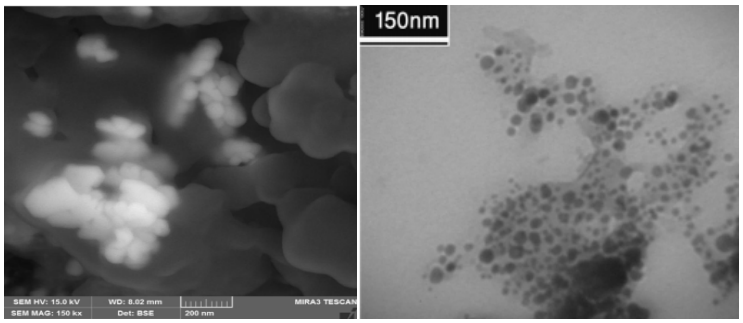

Figure 30. FESEM (left) and TEM (right) images of Ag/bone nanocomposite. Adapted with permission from ref. 215.

The synthesized material exhibited an excellent catalytic activity for the hydrolysis of a variety of arylcyanamides into the corresponding N-arylureas, and it could be recycled up to five times with no loss of performance. Notably, the reaction was carried out in the aqueous extract of *Myrica gale* as a solvent, thereby avoiding usage of additional media.[215]

4.2 Additional examples

Besides the examples detailed in the above paragraphs of section 4, several other studies on the synthesis of M-NPs stabilized in suspensions or immobilized on solids derived from biowastes have been described in the recent literature. Table 4 provides a summary of additional relevant examples.

Table 4. M-NPs stabilized in suspensions or immobilized on solids derived from biowastes

Entry	Biowaste from	Prepared nanomaterials	Ref.
1	Fish scales	Cu NPs	216
2	Lignocellulose	Ag NPs	217
3	Banana fruit extract	Au NPs	218
4	Vegetables	Au NPs	219
5	Food Industry	Zero valent Fe NPs	220
6	Wine dregs	Au and Ag NPs	221
7	Peach kernel shell	Ag NPs	222
8	Rice husks	Ru NPs on modified ceria	223
9	Chicken eggshell	CaO NPs	224
10	Eggshell	$CaCO_3$ nanofibrous	225

Conclusions

Generated annually on an impressive scale of billions of kilos, biowastes must enter a value chain crucial to rethink the planetary welfare in terms of circular economy, where the concept of sustainable growth is implemented through a closed loop for the recycle of any material or its transformation in other resources without harming and/or depleting the natural ecosystem. Biowastes can be radically transformed, either physically, chemically or biologically into a broad plethora of end use products and materials. This potential should be assessed on multiple beneficial aspects for the transition to a circular economy, these including the design of innovative products, the study of new business and market models, and even the promotion of changes in the consumers life style and behavior. However, due to the highly heterogenous nature of biowastes, identifying methods for their valorization is a challenging task not only to conceive the type of end- product or families of end-products, but also to characterize their properties. This review has been focused on the fabrication of biowaste-derived nanomaterials, starting from a selection of largely available sources as collagen, chitin and chitosan, hydroxyapatites and bio-silica/silicates, and other C-based feedstocks for bioplastics and nanocarbon structures to be used as such or as supports for metal nanoparticles. Perspectives for the applications of these materials span on most varied sectors from the biomedical in drug delivery and tissue engineering, to the environmental remediation, catalysis, electronics, energy storage, etc., and they are contributing drivers to enhance scientific and technological knowledge in these fields. However, many of such investigations are still at an early stage and need to be expanded beyond the discovery of a novel procedure or process, to an in-depth analysis of both technical aspects and socio-ecological boundaries including optimization of purification protocols, extraction yields, up-scaling issues, energy balance and costs, environmental emissions, and public acceptability and approval of new technologies.

References

[1] David Weedmark, https://sciencing.com/human-activities-affect-ecosystem-9189.html, Updated March 09, 2018

[2] http://ec.europa.eu/environment/waste/compost/index.htm, Last updated: 09/06/2016

[3] (a) M. M. Tun, D. Juchelková, H. Raclavská, V. Sassmanová *Energies* 2018, **11**, 3183; (b) http://web.unep.org/ourplanet/september-2015/unep-publications/global-waste-management-outlook

[4] D. Hoornweg, P. Bhada-Tata, What a Waste: *A Global Review of Solid Waste Management*; Urban Development Series Knowledge Papers; The World Bank Group: Washington, DC, USA, 2012; pp. 1–98

[5] From Waste to Value: Valorisation Pathways for Organic Waste Streams in Circular Bioeconomies, Eds**:** Antje Klitkou, Arne Fevolden; Taylor & Francis, 2019.

[6] (*a*) J. A. Bennett, K. Wilson, A. F. Lee, *J. Mater. Chem. A*, 2016, **4**, 3617-3637; (*b*) D. Rodriguez-Padron, A. R. Puente-Santiago, A. Caballero, A. M. Balu, A. A. Romero, R. Luque, *Nanoscale*, 2018, **10**, 3961-3968; (*c*) W. Ouyang, J.M. Reina, E. Kuna, A. Yepez, A.M. Balu, A. A. Romero, J. C. Colmenares, R. Luque, *J. Environ. Manage*., 2017, **203**, 768-773; (*d*) R. Luque, *Curr. Green Chem*., 2015, **2**, 90-95.

[7] J. Cai, N. Hishamunda *FAO Aquaculture Newsletter* **2013**, 51, 34–36, and *FAO Aquaculture Newsletter* 2018, **58**, 49–51

[8] The state of the World fisheries and aquaculture, meeting the sustainable development goals, Food and Agriculture Organization of the United Nations, Rome 2018, **ISBN 978-92-5-130562-1**

[9] G. Caruso, *J Fisheriessciences.com* 2016, **10**, 12-015.

[10] J. Guillen, S. J. Holmes, N. Carvalho, J. Casey, H. Dörner, M. Gibin, A. Mannini, P. Vasilakopoulos, A. Zanzi *Sustainability* 2018, **10**, 900.

[11] F. M. Kerton, Y. Liu, K. W. Omari, K. Hawboldt, *Green Chem.*, 2013, **15**, 860-871.

[12] K. Jayathilakan, K. Sultana & K. Radhakrishna, A. S. Bawa *J. Food Sci Technol*. 2012, **49**, 278–293

[13] S. Maqsood, S. Benjakul, A. Kamal-Eldin *Recent Pat Food Nutr Agric.* 2012, **4**, 141-7.

[14] BBI work plan 2018, topic identifier BBI.2018.SO1.R1: http://ec.europa.eu/research/participants/portal/desktop/en/opportunities/h2020/topics/bbi.2018.so1.r1.html, last access January 24th, 2019.

[15] M. Ahmaruzzaman, *Prog. Energy Combust. Sci.*, 2010, **36**, 327-363.

[16] J. M. Kurola, M. Arnold, M. H. Kontro, M. Talves, M. Romantschuk *Biores. Technol.* 2011, **102**, 5214–5220

[17] H. Raclavska, D. Juchelkova, V. Roubicek, D. Matysek *Fuel Proc. Technol*. 2011, **92**, 13–20

[18] J. Zuwala, M. Sciazko *Biomass Bioenergy* 2010, **34**, 1165-1174

[19] Z. Gogebakan, Y. Gogebakan, N. Selcuk, E. Selcuk, *Bioresour. Technol*. 200**9**, **100**, 1033–103

[20] N. M. Sigvardsen, L. M. Ottosen *Cem. Concr. Compos*. 2019, **95**, 25–32

[21] Z. T. Yao, X. S. Ji, P. K. Sarker, J. H. Tang, L. Q. Ge, M. S. Xia, Y. Q. Xi *Earth-Sci. Rev.* 2015, **141**, 105–121

[22] G. Xu, X. Shi *Resour. Conserv. Recy.* 2018, **136**, 95–109

[23] H. Chen Applications of Lignocellulose Biotechnology in Other Industries. In: Biotechnology of Lignocellulose; 2014, Springer, Dordrecht

[24] Lignocellulosic Biomass Production and Industrial Applications, A. Kuila, V. Sharma, Ed.; Scrivener Publishing, Wiley, 2017.

[25] B. Padrino, M. Lara-Serrano, S. Morales-delaRosa, J. M. Campos-Martín, J. L. García Fierro, F. Martínez, J. A. Melero, D. Puyol *Front. Bioeng. Biotechnol*. 2018, **6**, 119

[26] A. Duque, P. Manzanares, M. Ballesteros *Renew. Energy* 2017, **114**, 1427-1441

[27] W. Jianga, A. Kumar, S. Adamopoulos *Ind. Crops Prod*. 2018, **124**, 325–342

[28] F. G. Gachango, K. S. Ekmann, J. Frørup, S. M. Pedersen *Aquaculture* 2017, **479**, 265–272

[29] A. W. Lipkowski, B. Gajkowska, A. Grabowska, K. Kurzepa *Polimery* 2009, **54**, 386-388.

[30] M. Gonzalo, C. M. Jespersen, K. Jensen, S. Støier, L. Meinert 62nd International Congress of Meat Science and Technology, 14-19th August 2016, Bangkok, Thailand

[31] http://www1.bio.ku.dk/projects/keratin2protein/; last access January 25, 2019

[32] M.-H. Wonga, W.-Y. Mo, W-M. Choi, Z. Cheng, Y.-B. Man *Environ. Pollut*. 2016, **219**, 631-638

[33] Nitrogen inputs to agricultural soils from livestock manure, New statistics, Integrated Crop Management, FAO, Rome, Vol. 24, 2018; ISBN 978-92-5-130024-4

[34] I. M. Nasir, T. I. Mohd Ghazi, R. Omar *Eng. Life Sci.* 2012, **12**, 258–269

[35] E. Monteiro, V. Mantha, A. Rouboa *Renew. Energy* 2011, **36**, 627-631

[36] C. Cavinato, F. Fatone, D. Bolzonella, P. Pavan *Biores. Technol*. 2010, **101**, 545–550

[37] C. Zhang, G. Xiao, L. Peng, H. Su, T. Tan *Biores. Technol*. 2013, **129**, 170–176

[38] L. Castrillón, Y. Fernández-Nava, P. Ormaechea, E. Marañón *Biores. Technol.* 2013, **27**, 312–317

[39] H. Tian, N. Duan, C. Lin, X. Li, M. Zhong *J. Biosci. Bioeng*. 2015, **120**, 51-57

[40] S. A. Neshat, M. Mohammadi, G. D. Najafpour, P. Lahijani *Renew. Sustainable Energy Rev*. 2017, **79**, 308–322

[41] S. Astals, R. Musenze, X. Bai, S. Tannock, S. Tait, S. Pratt, P.D. Jensen *Biores. Technol*. 2015, **181**, 97–104
[42] S. Yin, R. Dolan, M. Harris, Z. Tan *Biores. Technol*. 2010, **101**, 3657–3664
[43] A. Dimitriadis, S. Bezergianni *Renew. Sustainable Energy Rev*. 2017, **68**, 113–125
[44] http://www.worldbank.org/en/topic/urbandevelopment/brief/solid-waste-management, last access, January 30, 2019
[45] D. Hoornweg, P. Bhada-Tata WHAT A WASTE, A Global Review of Solid Waste Management, Urban Development Series, Chapt. 5; World Bank, Washington, DC USA, 2012,
[46] S. Suthar, P. Singh *Sustainable Cities Soc*. 2015, **14**, 56–63
[47] B. A. Hakami, E.-S. Sedek Abu Seif *Int. Res. J. Environ. Sci.* 2015, **4**, 1-10
[48] P. Williams. The composition of household waste at the kerbside in 2014-15, Zero Waste Scotland, zerowastescotland.org.uk/content/contact-form, last access, January 30, 2019
[49] E. Imbert *Open Agric*. 2017, **2**, 195–204
[50] R. Arneil, D. Arancon, C. Sze Ki Lin, K. M. Chan, T. H. Kwan, R. Luque *Energy Sci. Eng*. 2013, **1**, 53-71
[51] F. Girotto, L. Alibardi, R. Cossu *Waste Manag*. 2015, **45**, 32–41
[52] T. I. J. Dugmore, J. H. Clark, J. Bustamante, J. A. Houghton, A. S. Matharu *Top Curr Chem (Z)*, 2017, **375**, 46
[53] V. dos Santos, R. N. Brandalise, M. Savaris, Engineering of Biomaterials, Biomaterials: characteristics and properties, Springer AG, 2017
[54] J. Park, R. S. Lakes Biomaterials: An Introduction, Springer Science & Business Media, 2007
[55] M. C. Gómez-Guillén, B. Giménez, M. E. López-Caballero, M. P. Montero *Food Hydrocolloid* 2011, **25**, 1813-1827
[56] O. Pasvolsky, R. Umalsky, Y. Naparstek, A. Y. Hershko, in Anticollagen Antibodies, Autoantibodies, 3rd Ed.; Eds.: Y. Shoenfeld, P. L. Meroni, M. E. Gershwin, Elsevier, 2014
[57] C. H. Lee, A. Singla, Y. Lee Int. J. Pharm. 2001, **221**, 1–22
[58] R. Parenteau-Bareil, R. Gauvin, F. Berthod *Materials* 2010, **3**, 1863-1887
[59] C. Y. Hsiao, C. H. Chou, H. W. Sun, J. N. Seah, EcoDynamic BioLab, Taipei (TW), US 7,396,912 B2 (Jul. 8, 2008)
[60] T. Nagai, N. Suzuki *Food Chem*. 2000, **68**, 277-281
[61] Y. Nomura, H. Sakai, Y. Ishii, K. Shirai *Biosci. Biotech. Biochem*. 1996, **60**, 2092-2094
[62] K.-M. Song, S. K. Jung, Y. H. Kim, Y. E. Kim, N. H. Lee *Food Bioprod. Process*. 2018, **110**, 96–103
[63] G. K. S. Arumugam, D. Sharma, R. M. Balakrishnan, J. B. P. Ettiyappan, *Sust. Chem. Pharm.*, 2018, **9**, 19-26.
[64] N. Muhammad, G. Gonfa, A. Rahim, P. Ahmad, F. Iqbala, F. Sharif, A. S. Khan, F. U. Khan, Z. U. H. Khan, F. Rehman, I. U. Rehman, *J. Mol. Liq.*, 2017, **232**, 258-264.
[65] P. G. Kumar, T. Nidheesh, K. Govindaraju, Jyoti, P. V. Suresh, *J. Sci. Food Agric.*, 2016, **97**, 1451-1458.
[66] C. Y. Huang, J. M. Kuo, S. J. Wub, H. T. Tsai, *Food Chem.*, 2016, **190**, 997-1006.
[67] C. K. S. Pillai, W. Paul, C. P. Sharma *Progr. Polymer Sci.* 2009, **34**, 641–678
[68] L. G. Baker, C. A. Specht, M. J. Donlin, J. K. Lodge *Eukaryotic Cell* 2007, **6**, 855–867
[69] A. Verlee, S. Mincke, C. V. Stevens, *Carbohydr. Polym.*, 2017, **164**, 268-283.
[70] C. Peniche, W. Argüelles-Monal, F. M. Goycoolea Chitin and Chitosan: Major Sources, Properties and Applications, In Monomers, Polymers and Composites from Renewable Resources; Eds: M. N. Belgacem, A. Gandini, Elsevier, 2008.
[71] R. Jayakumar, M. Prabaharan, P. T. Sudheesh Kumar, S. V. Nair, H. Tamura *Biotechnol. Adv*. 2011, **29**, 322–337
[72] S. Gopi, P. Balakrishnan, C. Divya, S. Valic, E. G. Bajsic, A. Pius and S. *Thomas, New J. Chem.,* 2017, **41**, 12746-12755.
[73] C. C. Satam, C. W. Irvin, A. W. Lang, J. C. R. Jallorina, M. L. Shofner, J. R. Reynolds, J. Carson Meredith *ACS Sustainable Chem. Eng.* 2018, **6**, 10637−10644
[74] F. Ding, H. Deng, Y. Du, X. Shi, Q. Wang *Nanoscale* 2014, **6**, 9477-
[75] Y. Zou, E. Khor, *Carbohydr. Polym.* 2009, **77**, 516-525
[76] E. Castagnino, M. F. Ottaviani, M. Cangiotti, M. Morelli, L. Casettari, R. A Muzzarelli *Carbohydr. Polym.* 2008, **74**, 640-647
[77] H. Liu, Q. Yang, L. Zhang, R. Zhuo, X. Jiang *Carbohydr. Polym.* 2016, **137**, 600-607
[78] N. Pacheco, M. Garnica-Gonzalez, M. Gimeno, E. Bárzana, S. Trombotto, L. David, K. Shirai, *Biomacromolecules*, 2011, **12**, 3285-3290.

[79] R. S. C. M. de Queiroz Antonino, B. R. P. L. Fook, V. A. de Oliveira Lima, R. Í. de Farias Rached, E. P. N. Lima, R. J. da Silva Lima, C. A. P. Covas, M. V. L. Fook, *Mar. drugs*, 2017, **15**, 141.
[80] X. Chen, H. Yang, Z. Zhong, N. Yan, *Green Chem*., 2017, **19**, 2783-2792
[81] E. Khor, L. Y. Lim *Biomaterials* 2003, **24**, 2339–2349
[82] V. K. Thakur, M. K. Thaku *ACS Sustainable Chem. Eng*. 2014, **2**, 2637−2652
[83] I. Younes, M. Rinaudo *Mar. Drugs* 2015, **13**, 1133-1174
[84] P. Kanmani, J. Aravind, M. Kamaraj, P. Sureshbabu, S. Karthikeyan *Biores. Technol*. 2017, **242**, 295–303
[85] J. Liang, H. Yan, P. Puligundla, X. Gao, Y. Zhou, X. Wan *Food Hydrocolloid* 2017, **69**, 286-292
[86] Y. Yan, X. Zhang, C. Li, Y. Huanga, Q. Dinga, X. Pang, *Appl. Surf. Sci.* 2015, **332**, 62–69
[87] A. Szcześ, L. Hołysz, E. Chibowski *Adv. Colloid Interfac*. 2017, **249**, 321–330
[88] M. Akram, R. Ahmed, I. Shakir, W. Aini, W. Ibrahim, R. Hussain *J. Mater. Sci.* 2014, **49**, 1461–1475
[89] N. A. M. Barakat, M. S. Khil, A. M. Omran, F. A. Sheikh, H. Y. Kim, *J. Mater. Process. Technol.,* 2009, **209**, 3408-3415.
[90] S. Kongsri, K. Janpradit, K. Buapa, S. Techawongstien, S. Chanthai *Chem. Eng. J.* 2013, **215–216**, 522–532
[91] W. Pon-Ona, P. Suntornsaratoon, N. Charoenphandhu, J. Thongbunchoo, N. Krishnamra, I. M. Tang *Mater. Sci. Eng. C* 2016, **62**, 183–189
[92] B. Ratna Sunil, M. Jagannatham *Mater. Lett.* 2016, **185**, 411–414
[93] P. Shi, M. Liu, F. Fan, C. Yu, W. Lu, M. Du, *Mater. Sci. Eng. C,* 2018, **90**, 706-712.
[94] F. Heidari, M. E. Bahrololoom, D. Vashaee, L. Tayebi *Ceram. Int.* 2015, **41**, 3094–3100
[95] S. Pokhrel *Adv. Chem. Eng. Sci*. 2018, **8**, 225-240
[96] T. Iwata *Angew. Chem. Int. Ed*. 2015, **54**, 3210–3215
[97] OECD, 2013. Policies for Bioplastics in the Context of a Bioeconomy. http://search.oecd.org/officialdocuments/publicdisplaydocumentpdf/?cote=DSTI/STP/BIO(2013)6/FINAL&docLanguage=En (last access February 11th, 2019).
[98] https://www.european-bioplastics.org/global-market-for-bioplastics-to-grow-by-20-percent/ (last access February 11th, 2019).
[99] P. Morone, V. E. Tartiu, P. Falcone, *J. Clean. Prod.,* 2015, **90**, 43-54.
[100] C.S. Araújo, A.M.C. Rodrigues, M.R.S. Peixoto Joele, E.A.F. Araújo, L.F.H. Lourenço, *Food Pack. Shelf Life*, 2018, **16**, 23-30
[101] I. S. Bayer, S. G. Puyol, J. A. Heredia-Guerrero, L. Ceseracciu, F. Pignatelli, R. Ruffilli, R. Cingolani, A. Athanassiou, *Macromolecules,* 2014, **47**, 5135-5143.
[102] G. Perotto, L. Ceseracciu, R. Simonutti, U. C. Paul, S. Guzman-Puyol, T. N. Tran, I. S. Bayer, A. Athanassiou, *Green Chem.,* 2018, **20**, 894-902
[103] T. Mekonnen, P. Mussone, H. Khalil, D. Bressler *J. Mater. Chem. A*, 2013, **1**, 13379–13398
[104] K. Y. Nandiwale, S. P. Borikar, V. V. Bokade *Clean–Soil, Air, Water* 2015, **43**, 927–931
[105] M. Auriemma, A. Piscitelli, R. Pasquino, P. Cerruti, S. Angelini, G. Scarinzi, M. Malinconico, N. Grizzuti, AIP Conf. Proc. 2015, **1965**, 020026
[106] K. W. Lee, J. W. Chung, S.-Y. Kwak *ACS Sustainable Chem. Eng*. 2018, **6**, 9006−9017
[107] Y. Yang, J. Huang, R. Zhang, J. Zhu *Mater. Design* 2017, **126**, 29–36
[108] L. A. Derry, A. C. Kurtz, K. Ziegler, O. A. Chadwick *Nature* 2005, **433**, 728−731
[109] C. M Zaremba, G. D Stucky *Curr. Opin. Solid St. M*. 1996, **1**, 425-429
[110] FAO, Rice market monitor, http://www.fao.org/3/I9243EN/i9243en.pdf, last access February 14, 2019
[111] W. Wang, J. C. Martin, X. Fan, A. Han, Z. Luo, L. Sun *ACS Appl. Mater. Interfaces* 2012, **4**, 977−981
[112] K. G. Patel, R. R. Shettigar, N. M. Misra J. *Adv. Agric. Technol*. 2017, **4**, 274-279
[113] Y. Shen *J. Agric. Food Chem*. 2017, **65**, 995−1004
[114] S. Praneetha and A. Vadivel Murugan, *ACS Sustainable Chem. Eng.,* 2015, **3**, 224-236.
[115] R. Choudhary, S. Koppala, S. Swamiappan, *J. Asian Ceram. Soc.*, 2015, **3**, 173-177.
[116] W. You, M. Hong, H. F. Zhang, Q. Wu, Z. Zhuang, Y. Yu, *Phys. Chem. Chem. Phys.,* 2016, **18**, 15564-15573.
[117] F. A. Sheikh, M. A. Kanjwal, J. Macossay, M. A. Muhammad, T Cantu, N. A. M. Barakat, H. Y. Kim, *J. Biomater. Tissue. Eng*., 2011, **1**, 194-197
[118] J. Wasswa, J. Tang, X. Gu, *Food Rev. Int*., 2007, **23**, 159-174

[119] M.-M. Chen, Y.-Q. Huang, H. Guo, Y. Liu, J.-H. Wang, J.-L. Wu, Q.-Q. Zhang, *J. Appl. Polym. Sci*., 2014, **131**, 40998;
[120] R. D. Thanoon, R. Subramaniam, E. A. Makky, M. M. Yusoff, *Jordan J. Biol. Sci*., 2018, **11**, 17-22
[121] H. M. P. M. Jose, P. Murugesan, M. Arumugam, K. Mahesh Kumar, *Int. J. Pharm. Pharm. Sci*., 2014, **6**, 654-657;
[122] P. Terzioğlu, H. Öğüt, A. Kalemtas, *Mater. Sci. Eng. C*, 2018, **91**, 899-911
[123] S. Iswariya, P. Velswamy, T. S. Uma, *J. Polym. Environ*., 2018, **26**, 2086-2095;
[124] E. I. Akpan, S. O. Adeosun, G. I. Lawal, S. A. Balogun, X. D. Chen, *J. Nat. Fibers*, 2016, **13**, 103-124
[125] T. Nagai, E. Yamashita, K. Taniguchi, N. Kanamori, N. Suzuki, *Food Chem*., 2001, **72**, 425-429;
[126] L. Xiaoying, F. Yongbin, G. Dachun, C. Wei, *Key Eng. Mater*., 2007, **342-343**, 213-216
[127] L.S. Senaratne, P.-J. Park, S.-K. Kim, *Bioresour. Technol*., 2006, **97**, 191-197;
[128] G. S. Kumar, E. K. Girija, *Ceram. Int*., 2013, **39**, 8293-8299;
[129] S. Sankar, S. Sekar, R. Mohan, S. Rani, J. Sundaraseelan, T. P. Sastry, *Int. J. Biol. Macromol*., 2008, **42**, 6-9;
[130] A.-R. Ibrahim, W. Wei, D. Zhang, H. Wang, J. Li, *Mater. Lett*., 2013, **110**, 195-197
[131] A. Muthuvel, T. Ajithkumar, T. Balasubramanian, *J. Appl. Biol. Sci*., 2011, **5**, 7-10
[132] W.-K. Liu, B.-S. Liaw, H.-K. Chang, Y.-F. Wang, P.-Y. Chen, *JOM*, 2017, **69**, 713-718;
[133] A. Veeruraj, M. Arumugam, T. Ajithkumar, T. Balasubramanian, *J. Mater. Sci. Mater. Med*., 2012, **23**, 1729-1738
[134] S. Thammahiwes, S.-A. Riyajan, K. Kaewtatip, *J. Polym. Environ*., 2018, **26**, 1775-1781
[135] Y.-P. Chen, C.-H. Liang, H.-T. Wu, H.-Y. Pang, C. Chen, G.-H. Wang, L.-P. Chan, *J. Food Sci. Technol*., 2018, **55**, 2310-2317;
[136] K. P. Kota, S. S. Shaik, R. K. Kota, A. P. Karlapudi, *Int. J. Pharm. Sci. Rev. Res*., 2014, **27**, 373-375
[137] A. B. Muley, S. A. Chaudhari, K. H. Mulchandani, R. S. Singhal, *Int. J. Biol. Macromol*., 2018, **111**, 1047-1058;
[138] S. Thammahiwes, S.-A. Riyajan, K. Kaewtatip, *J. Cereal. Sci*., 2017, **75**, 186-191
[139] T. Kleekayai, W. Suntornsuk, *World J. Microbiol. Biotechnol*., 2011, **27**, 1145-1154
[140] C.-S. Wu, *Polym. Degrad. Stab*., 2012, **97**, 64-71
[141] M. Ashokkumar, K. M. Sumukh, R. Murali, N. T. Narayanan, P. M. Ajayan, P. Thanikaivelan, *Carbon*, 2012, **50**, 5574-5582
[142] A. L. Wong, H. Chua, W. H. Lo, P. H. F. Yu, *Water Sci. Technol*., 2018, **41**, 55-59
[143] S. Kumari, R. Rath, A. S. H. Kumar, T. N. Tiwari, *Environ. Technol. Innov*., 2015, **3**, 77-85
[144] T. M. A. Moro, J. L. R. Ascheri, J. A. R. Ortiz, C. W. P. Carvalho, A. Meléndez-Arévalo, *Food Bioprocess Technol*., 2017, **10**, 1798-1808
[145] S.-L. Wang, W.-N. Tseng, T.-W. Liang, *Biodegradation*, 2011, **22**, 939-948
[146] M. Ben, T. Mato, A. Lopez, M. Vila, C. Kennes, M. C. Veiga, *Water Sci. Technol*., 2011, **63**, 1196-202
[147] V. L. Pachapur, K. Guemiza, T. Rouissi, S. J. Sarma, S. K. Brar, *J. Chem. Technol. Biotechnol*., 2016; **91**, 2331-2339;
[148] H. Chen, L. Zhao, X. Wang, X. He, W. Fang, X. Wang, F. Wang, *Ceram. Int*., 2015, **41**, 6089-6097
[149] C. Webster, O. Onokpise, M. Abazinge, J. Muchovej, E. Johnson, C. Louime, *Amer. J. Environ. Sci*., 2014, **10**, 357-362
[150] B. I. Ugheoke, O. Mamat, *Int. J. Mater. Eng. Innov*., 2012, *3*, 139-155.
[151] M.-T. Yen, J.-H. Yang, J.-L. Mau, *Carbohydr. Polym*., 2009, **75**, 15-21
[152] S. Collazo-Bigliardi, R. Ortega-Toro, A. Chiralt Boix, *Carbohydr. Polym.*, 2018, **191**, 205-215
[153] N. Rakkhumkaew, C. Pengsuk, *Food. Sci. Biotechnol*., 2018, **27**, 1201-1208;
[154] B. R. Rampazzo, D. Alkan, S. Gazzotti, M. A. Ortenzi, G. Piva, L. Piergiovanni, *Packag. Technol. Sci.*, 2017, **30**, 645-661
[155] J. Ma, C. Xin, C. Tan, *Int. J. Biol. Macromol*., 2015, **80**, 547-556
[156] D. Pavan Kumar, M. V. Chandra, K. Elavarasan, B. A. Shamasundar, *Int. J. Food. Prop.*, 2017, **20**, S2612-S2625
[157] J. J. Vilatela, D. Eder *ChemSusChem* 2012, **5**, 456-478
[158] S. K. Rastogi, A. Kalmykov, N. Johnson, T. Cohen-Karni *J. Mater. Chem. B* 2018, **6**, 7159-7178
[159] C. Tang, M.-M. Titirici, Q. Zhang *J. Energy Chem*. 2017, **26**, 1077–1093

[160] M. Arugula, A. Simonian *J. Solid State Sci. Technol*. 2016, **5**, M3045-M3053
[161] M. Zhang, K. P. Annamalai, L. Liu, T. Chen, Y. Tao *Recent Innov. Chem. Eng*. 2016, **9**, 4-19
[162] A. Bhati, G. K. M. Tripathi, A. Singh, S. Sarkar, S. K. Sonkar *New J. Chem.,* 2018, **42**, 16411--16427
[163] S. D. Lakshmi, P. K. Avti, G. Hegde *Nano-Structures & Nano-Objects* 2018, **16**, 306–321
[164] M. Ashokkumar, N. T. Narayanan, A. L. M. Reddy, B. K. Gupta, B. Chandrasekaran, S. Talapatra, P. M. Ajayan, P. Thanikaivelan *Green Chem*., 2012, **14**, 1689–1695
[165] M. Ashokkumar, A. C. Chipara, N. T. Narayanan, A. Anumary, R. Sruthi, P. Thanikaivelan, R. Vajtai, S. A. Mani, P. M. Ajayan *ACS Appl. Mater. Interfaces* 2016, **8**, 14836−14844
[166] B. Telay Mekonnen, A. Meiyazhagan, M. Ragothaman, C. Kalirajan, T. Palanisamy *J. Clean. Prod.* 2019, **210**, 190-199
[167] E. Thompson, A. E. Danks, L. Bourgeois, Z. Schnepp, *Green Chem*., 2015, **17**, 551-556
[168] A. Zuliani, M. J. Munoz-Batista, R. Luque, *Green Chem.*, 2018, **20**, 3001-3007.
[169] A. Kumar, G. Hegde, S. A. B. A. Manaf, Z. Ngaini, K. V. Sharma *Chem. Commun*.,2014, **50**, 12702--12705
[170] G. A. M. Ali, S. A. B. A. Manaf, A. Divyashree, K. F. Chong, G. Hegde *J. Energy Chem*. 2016, **25**, 734–739
[171] J. B. Essner, G. A. Baker *Environ. Sci.: Nano*, 2017, **4**, 1216–1263
[172] R. Wang, K.-Q. Lu, Z.-R. Tang, Y.-J. Xu *J. Mater. Chem. A*, 2017, **5**, 3717–3734
[173] S. Cailotto, R. Mazzaro, F. Enrichi, A. Vomiero, M. Selva, E. Cattaruzza, D. Cristofori, E. Amadio, A. Perosa *ACS Appl. Mater. Interfaces* 2018, **10**, 40560−40567
[174] X. Zhang, M. Jiang, N. Niu, Z. Chen, S. Li, S. Liu, J. Li *ChemSusChem* 2018, **11**, 11– 24
[175] R. Das, R. Bandyopadhyay, P. Pramanik *Mater. Today Chem.* 2018, **8**, 96-109
[176] W. Lu, X. Qin, S. Liu, G. Chang, Y. Zhang, Y. Luo, A. M. Asiri, A. O. A. Youbi, X. Sun, *Anal. Chem.*, 2012, **84**, 5351-5357.
[177] W. Du, X. Xu, H. Hao, R. Liu, D. Zhang, F. Gao, Q. Lu, *Sci. China Ser. B* 2015, **58**, 863-870
[178] G. Wu, M. Feng, H. Zhan, *RSC Adv.*, 2015, **5**, 44636-44641
[179] Z. Wang, J. Yu, X. Zhang, N. Li, B. Liu, Y. Li, Y. Wang, W. Wang, Y. Li, L. Zhang, ACS *Appl. Mater. Interfaces* 2016, **8**, 1434 –1439.
[180] R. Liu, J. Zhang, M. Gao, Z. Li, J. Chen, D. Wu, P. Liu, *RSC Adv*. 2015, **5**, 4428 –4433.
[181] A. Suryawanshi, M. Biswal, D. Mhamane, R. Gokhale, S. Patil, D. Guin, S. Ogale, *Nanoscale* 2014, **6**, 11664–11670
[182] Y. Li, W. Liao, Z. Li, T. Feng, L. Sun, C. Guo, J. Zhang, J. Li *Carbon* 2017, **125**, 640-648
[183] C. Guo, R. Hu, W. Liao, Z. Li, L. Sun, D. Shi, Y. Li, C. Chen *Electrochimica Acta* 2017, **236**, 228–238
[184] P. Yang, J. Xie, C. Zhong, *ACS Appl. Energy Mater.,* 2018, **1**, 616-622.
[185] D. Yu, C. Chen, G. Zhao, L. Sun, B. Du, H. Zhang, Z. Li, Y. Sun, F. Besenbacher, M. Yu *ChemSusChem.* 2018, **11**, 1678-1685
[186] Y. Liu, Z. Xiao, Y. Liu, L.-Z. Fan *J. Mater. Chem. A*, 2018, **6**, 160–166
[187] H. Chen, G. Wang, L. Chen, B. Dai, F. Yu, *Nanomaterials,* 2018, **8**, 412.
[188] A. Jain, S. K. Tripathi, *J. Energy Storage*, 2015, **4**, 121-127
[189] G. Hegde, S. A. A. Manaf, A. Kumar, G. A. M. Ali, K. F. Chong, Z. Ngaini, K. V. Sharma, *ACS Sustainable Chem. Eng*., 2015, **3**, 2247-2253;
[190] Y. Ke, B. Garg, Y.-C. Ling, *RSC Adv*., 2014, **4**, 58329-58336
[191] Y. S. Yun, M. H. Park, S. J. Hong, M. E. Lee, Y. W. Park, H.-J. Jin, *ACS Appl. Mater. Interfaces*, 2015, **7**, 3684-3690;
[192] S. K. Sonkar, M. Roy, D. G. Babar, S. Sarkar, *Nanoscale*, 2012, **4**, 7670-7675
[193] Y. Li, X. Wang, M. Cao, *J. CO_2 Utilization*, 2018, **27**, 204-216;
[194] P. Z. Z. Ngu, S. P. P. Chia, J. F. Y. Fong, S. M. Ng, *New Carbon Mater*., 2016, **31**, 135-143
[195] O. F. Cruz, J. Silvestre-Albero, M. E. Casco, D. Hotza, C. R. Rambo, *Mater. Chem. Phys*., 2018, **216**, 42-46
[196] Ö. Güler, M. Boyrazlı, Ö. Başgöz, B. Bostancı, *Can. Metall. Q*., 2017, **56**, 349-359
[197] P. O. Patil, P. V. Bhandari, P. K. Deshmukh, S. S. Mahale, A. G. Patil, H. R. Bafna, K. V. Patel, S. B. Bari, *Res. Chem. Intermed*., 2017, **43**, 3757-3773
[198] H. Wang, X. Qiu, R. Zhong, F. Fu, Y. Qian, D. Yang, *Mater. Chem. Phys*., 2017, **199**, 193-202;
[199] I. L.A. Ouma, E. B. Naidoo, A. E. Ofomaja, *Eur. Phys. J. Appl. Phys*., 2017, **79**, 30401
[200] M. Khazaei, A. Khazaei, M. Nasrollahzadeh, M. R. Tahsil, *Tetrahedron*, 2017, **73**, 5613-4623

[201] Y. Wu, H. Wang, M. Cao, Y. Zhang, F. Cao, X. Zheng, J. Hu, J. Dong, Z. Xiao, *J. Nanosci. Nanotechnol*., 2015, **15**, 6495-6502.
[202] Y. Dahman, *Nanotechnology and Functional Materials for Engineers, Nanoparticles* (Ch. 5), Elsevier, 2017.
[203] M. Selva, A. Perosa, P. Canton *Curr. Org. Chem.*, 2017, **21**, 2445-2454
[204] A. Kraynov, T. E. Müller Concepts for the Stabilization of Metal Nanoparticles in Ionic Liquids, Applications of Ionic Liquids in Science and Technology; Ed: S. Handy, Intech, 2011.
[205] A. K. Mittal, Y. Chisti, U. C. Banerjee *Biotechnol. Adv*. 2013, **31**, 346–356
[206] N. Asmathunisha, K. Kathiresan *Colloids Surf. B: Biointerfac*. 2013, **103**, 283–287
[207] S. Iravani *Green Chem*., 2011, **13**, 2638-2650
[208] B. Baruwati, R. S. Varma *ChemSusChem* 2009, **2**, 1041 – 1044
[209] T.V.M. Sreekanth, S. Ravikumar, Y. R. Lee, *J. Mol. Recognit.,* 2016, **29**, 253-259.
[210] P. S. Devi, S. Banerjee, S. R. Chowdhury, G. S. Kumar, *RSC Adv*., 2012, **2**, 11578-11585.
[211] D. He, A. Ikeda-Ohno, D. D. Boland, T. D. Waite *Environ. Sci. Technol*. 2013, **47**, 5276-5284
[212] Y. Li, J. Y. Lan, J. Liu, J. Yu, Z. Luo, W. Wang, L. Sun, *Ind. Eng. Chem. Res.*, 2015, **54**, 5656-5663.
[213] M. J. Rak, T. Friščić, A. Moores, *Faraday Discuss.,* 2014, **170**, 155-167.
[214] M. Nasrollahzadeh, S. M. Sajadi, A. Hatamifard, *Appl. Catal. B Environ*., 2016, **191**, 209-227
[215] S. S. Momeni, M. Nasrollahzadeh, A. Rustaiyan, *J Colloid Interface Sci.*, 2017, **499**, 93-101.
[216] T. Sinha, M. Ahmaruzzaman, *Environ. Sci. Pollut. Res*., 2015, **22**, 20092-20100
[217] V. P. Manjamadha, K. Muthukumar, *Int. J. Nanosci*., 2016, **15**, 1660001
[218] G. K. Deokar, A. G. Ingale, *RSC Adv*., 2016, 6, 74620-74629
[219] R. Mythili, T. Selvankumar, P. Srinivasan, A. Sengottaiyan, J. Sabastinraj, F. Ameen, A. Al-Sabri, S. Kamala-Kannan, M. Govarthanan, H. Kim, *J. Mol. Liq*., 2018, **262**, 318-321
[220] S. Machado, J. P. Grosso, H. P. A. Nouws, J.T. Albergaria, C. Delerue-Matos, *Sci. Total Environ*., 2014, **496**, 233-240;
[221] N. González-Ballesteros, J. B. Rodríguez-González, M. C. Rodríguez-Argüelles, *J. Photochem. Photobiol. B*, 2018, **178**, 302-309
[222] B. Khodadadi, M. Bordbar, M. Nasrollahzadeh, *J. Colloid Interface Sci*., 2017, **493**, 85-93;
[223] O. B. Shawkataly, R. Jothiramalingam, F. Adam, T. Radhika, T. M. Tsao, M. K. Wang, *Catal. Sci. Technol*., 2012, **2**, 538-546
[224] P. R. Pandit, M.H. Fulekar, *J. Environ. Manage.*, 2017, **198**, 319-329
[225] A. Tavangar, B. Tan, K. Venkatakrishnan, *J Nanobiotechnology*, 2011, **9**, 1